Biomedicine & Pharmacotherapy 156 (2022) 113844

Contents lists available at ScienceDirect

Biomedicine & Pharmacotherapy

journal homepage: www.elsevier.com/locate/biopha

2-pentadecyl-2-oxazoline prevents cognitive and social behaviour impairments in the Amyloid β-induced Alzheimer-like mice model: Bring the α2 adrenergic receptor back into play

R. Infantino [a,1], S. Boccella [a,1], D. Scuteri [b,c,1], M. Perrone [a], F. Ricciardi [a], R.M. Vitale [d], R. Bonsale [a], A. Parente [e], I. Allocca [f], A. Virtuoso [f], C. De Luca [f], C. Belardo [a], P. Amodeo [d], V. Gentile [e], G. Cirillo [f], G. Bagetta [g], L. Luongo [a,h], S. Maione [a,h,*], F. Guida [a,**]

[a] Department of Experimental Medicine, Division of Pharmacology, University of Campania "L. Vanvitelli", 80138 Naples, Italy
[b] S. Anna Institute, Regional Center for Serious Brain Injuries, Crotone, Italy
[c] Pharmacotechnology Documentation and Transfer Unit, Preclinical and Translational Pharmacology, Department of Pharmacy, Health Science and Nutrition, University of Calabria, Rende (Cosenza), Italy, Regional Center for Serious Brain Injuries, Crotone, Italy
[d] Institute of Biomolecular Chemistry, National Research Council (ICB-CNR), Via Campi Flegrei 34, 80078 Pozzuoli, NA, Italy
[e] Department of Precision Medicine, Division of Biochemistry, Biophysics and General Pathology, University of Campania "Luigi Vanvitelli", Naples, Italy
[f] Laboratory of Morphology of Neuronal Networks and Systems Biology, Department of Mental and Physical Health and Preventive Medicine, University of Campania "Luigi Vanvitelli", 80138 Naples, Italy
[g] Preclinical and Translational Pharmacology, Department of Pharmacy, Health Science and Nutrition, University of Calabria, Rende, Cosenza, Italy
[h] IRCSS, Neuromed, 86077 Pozzilli, Italy

ARTICLE INFO

Keywords:
Amyloid β (1−42)
α2 adrenergic receptor
Alzheimer Disease
2-pentadecyl-2-oxazoline

ABSTRACT

The 2-pentadecyl-2-oxazoline (PEA-OXA) is a natural compound with protective action in neuro-inflammation. We have previously shown that PEA-OXA behaves as an α2 adrenergic receptor (α2AR) antagonist and a putative protean agonist on histamine H3 receptors. Recently, neuroinflammation and monoaminergic neurotransmission dysfunction has drawn particular attention in Alzheimer Disease (AD) pathophysiology. In this context, the objective of this study was to investigate the effects of the dual-acting PEA-OXA in an AD-like model in mice. A combined computational and experimental approach was used to evaluate the ability of PEA-OXA to bind α2A-AR subtype, and to investigate the effects of PEA-OXA treatment on neuropathological (behavioural and functional) effects induced by soluble Amyloid β 1–42 (sAβ1–42) intracerebroventricular injection. Computational analysis revealed the PEA-OXA ability to bind the α2A-AR, a pharmacological target for AD, in two alternative poses, one overlapping the Na+ binding site. *In vivo* studies indicated that chronic treatment with PEA-OXA (10 mg/kg, os) restored the cognitive (discriminative and spatial memory) deficits and social impairments induced by sAβ injection. Consistently, electrophysiological analysis showed a recovery of the long-term potentiation in the hippocampus (Lateral Entorhinal Cortex-Dentate Gyrus pathway), while neuroinflammation, i.e., increased pro-inflammatory cytokines levels and microglia cells density were reduced. These data provide the basis for further investigation of the pro-cognitive aptitude of PEA-OXA by proposing it as an adjuvant in the treatment in AD, for which the available pharmacological approaches remain unsatisfactory. Moreover, this study offers new future direction in research investigating the role of α2AR in neuropsychiatric illness and therapies.

1. Introduction

Alzheimer's disease (AD) is a very disabling neurodegenerative disease with progressive cognitive decline. It represents 60–70 % of cases of dementia and is the 7th leading cause of death globally [1,2]. AD carries permanent disability and a high comorbidity rate, with important health care costs [3]. Its high incidence is expected to increase over the years, given the progressive aging of the population [4]. The main

* Corresponding author at: Department of Experimental Medicine, Division of Pharmacology, University of Campania "L. Vanvitelli", 80138 Naples, Italy.
** Corresponding author.
[1] 1st authorship.

https://doi.org/10.1016/j.biopha.2022.113844
Received 12 September 2022; Received in revised form 3 October 2022; Accepted 6 October 2022
Available online 15 October 2022

pathophysiological mechanisms are strongly linked to the Amyloid β (1−42), (Aβ) cascade, which progressively leads to tau protein over-phosphorylation with the axons micro-tubular structure disorganization and, hence, the progressive neuronal loss [5,6]. Recent evidence indicates that, together with Aβ, hyper-phosphorylated tau has a synergistic pathophysiological role in synaptic remodeling, as well as in the recognized role of regulation of axonal cytoskeletal assembly. Furthermore, the neurofibrillary tangles themselves appear to undergo inter-synaptic trafficking with the consequent neurotoxic effect in different neuronal circuits. It seems important in the progression of the pathology, not only the neural and synapse loss, but the diffusion through the neural circuits of the hyper-phosphorylated tau or of the neurofibrillary tangles [7]. Aβ oligomers are derived from the amyloid precursor protein (APP), a neuroprotective protein under physiological conditions, which promotes survival, differentiation, and neurogenesis [8]. Areas with active neurogenesis such as the hippocampus, involved in learning and memory, are more precociously vulnerable to the toxic action of Aβ (1−42) [9,10]. Despite advances in understanding the pathophysiology of AD, drugs aimed at neutralizing or reducing Aβ accumulation, or even secretase inhibitors, have failed in humans. Thus, targets available remain neurotransmitter- and/or receptor-based [11–13].

Several neurotransmitter pathways are involved in the cognitive dysfunction of AD. In addition to a severe deficit in the cholinergic system, changes in GABA, glutamate, and biogenic amines have been highlighted [14]. Among them, noradrenergic and histaminergic transmissions attracted particular attention [15,16]. Indeed, noradrenaline and histamine are involved in neuroinflammatory phenomena, neurogenesis, and several key mechanisms related to cognition and neuroplasticity [17–20]. There is evidence of severe neurodegeneration in the locus coeruleus (LC) as well as functional alteration of noradrenergic receptors in the AD brain. The morpho-functional changes of the noradrenergic tone are closely correlated with some hallmarks of AD: the number of amyloid plaques, neurofibrillary tangles, and worsening of the clinical condition [21]. It has emerged over the years the link between α2-adrenergic receptors (α2AR) and the regulation they exert on cortical cholinergic transmission through their presynaptic hetero-receptor action [22,23]. This suggests how pharmacologically interesting it could be to modulate cholinergic tone, but also other neurotransmissions apart from noradrenergic itself, with selective α2AR subtype receptors drugs [24].

Among the receptor systems affected by AD pathology, the adrenergic system is the one that is increasingly gaining attention, in light of its involvement in memory formation, neurogenesis, and contribution to the progression of neurodegenerative changes upon AD [25,26]. There is evidence that blocking these receptors can exert neuroprotective, neurogenic, and Aβ-reducing effects, both in vivo and in vitro [27,28]. These effects are not only due to a modulation of the releases of different neurotransmitters but also to their presence on the astrocytes where they actively contribute to the regulation of the metabolism and other essential functions linked to neuronal well-being [29].

Recently, an oxazoline derivative of aliamide palmitoylethanolamide, the 2-Pentadecyl-2-oxazoline (PEA-OXA), was isolated and extracted from green and roasted coffee beans and may, thus represents a “dietary molecule”. This dual-acting compound showed the ability to negatively modulate the activity of the N-Acylethanolamine Acid Amidase (NAAA), maximizing the action of PEA, and exerting neuroprotective and anti-inflammatory properties [30]. In addition, a receptor-based activity of PEA-OXA has been recently demonstrated. Specifically, α2 antagonism and histaminergic modulation through H3 receptors putative protean agonism have been described, suggesting a pro-cognitive potential in different animal models, specifically in cognitive impairments related to neuropathic pain and traumatic brain injury [31,32].

Considering these observations and previous results, this study aimed to test the ability of PEA-OXA to prevent and/or restore cognitive impairment in an AD-like mouse model, through a multidisciplinary approach.

2. Materials and methods

2.1. Animals

A total number of 200 male CD1 mice (Envigo, Italy), 7–8 weeks old were used for the study. Mice were housed three per cage under controlled temperature (24 ± 1 °C) and humidity (55 ± 10 %) with a 12-hour light-dark cycle with food and water ad libitum.

2.2. Study approval

Experimental procedures were approved by the Animal Ethics Committee of the University of Campania L. Vanvitelli. Animal care was under the Dlgs 26/14 of the Italian law implementing the European Community (E.C. L358/1 18/ 12/86) guidelines about the experimental use of animals, minimizing the number and the suffering of animals to the essentials for achieving scientifically unbiased results, following ARRIVE guidelines.

2.3. Drugs and chemicals

2-Pentadecyl-2-oxazoline (PEA-OXA) was kindly provided by EPI-TECH Group SpA, Saccolongo (PD). PEA-OXA was dissolved in 2.5 % Carboxymethyl cellulose (CMC) for oral use, daily administered for 7–14 days, by gavage 2.0 at a dosage of 10 mg/kg in a final dose volume of 100 μl. For the acute challenge PEA-OXA was dissolved in Kolliphor 5 % (Sigma-Aldrich) in a final dose volume of 100 μl, and intraperitoneally (i.p.) administered 1 h or 24 h before behavioural and electrophysiological evaluations. The same volume of 2.5 CMC or 5 % Kolliphor was used as vehicle control. The dosage of PEA-OXA was chosen based on previous studies of our and other laboratories [30–33].

Soluble Amyloid-β (1−42) human peptide (sAβ) was purchased by Tocris (Bristol, UK). Stock solution aliquots were obtained by making a 1 mM DMSO solution to first dissolve pre-aggregates and then diluted to a 40 μM concentration with double-distilled water [34]. Finally, aliquots were stored at − 20 °C. The injected solution was freshly prepared before the surgery diluting the stock solution with sterile double-distilled water (vehicle) rising at a concentration of 4 μM as previously described [35,36].

2.4. Computational Methods for PEA-OXA binding site

Starting ligand geometry was built with UCSF Chimera 1.17 [37] and energy was minimized as already described [31]. Docking studies were performed with AutoDock 4.2 [38] and Autodock Vina [39], by using a homology model of rat α2A, built using the available x-ray structure of the human orthologue (PDB id: 6kux) as a template with the MODELLER v10.1 program [40]. 50 Homology models were built using the alignment shown in Suppl. Fig. 1. The long, flexible, intracellular loop ILC3 connecting helix 5 to helix 6 was shortened to eight residues. The best model in terms of both Modeller Objective Function and Dope score was selected for the subsequent docking calculations. Docking runs were carried out by either keeping fixed the whole protein or alternately allowing the rotation of selected residues, namely Trp387, Phe391, and Tyr416. Both proteins and ligands were processed with AutoDock Tools (ADT) package version 1.5.7 [38] to merge non-polar hydrogens and calculate Gasteiger charges. Grids for docking evaluation, with a spacing of 0.375 Å and 70 × 60 x 60 points centered on the binding site, were generated using the program AutoGrid 4.2 included in Autodock 4.2 distribution. Docking runs were carried out using the Lamarckian genetic algorithm (LGA), according to the protocol already published [41].

The complex selection was based on binding energy and the cluster population was completed by the addition of all hydrogen atoms and

underwent energy minimization. The energy-minimized complexes were embedded in a pre-equilibrated palmitoyl-oleoyl-phosphatidylcholine (POPC) lipid bilayer and solvated in an aqueous medium using the CHARMM-GUI web interface (http://www.charmm-gui.org). Potassium and chloride ions were added to ensure electric neutrality and 0.15 M ionic strength. MD simulations were carried out with the PMED. CUDA module of the Amber20 package [42], using lipid 14 (lipids), ff14SB force (proteins), and gaff (ligand) force field parametrization. The system underwent 10,000 steps of energy minimization keeping the solute atoms harmonically restrained to their starting positions (Kr = 10 kcal mol^{-1} $Å^{-1}$). The system was gradually heated to 100 K for 500 ps keeping fixed solute and lipid atoms using a Langevin thermostat, followed by subsequent heating up to the final temperature of 310 K for 1 ns, keeping fixed the solute and lipid atoms, using an anisotropic Berendsen weak-coupling barostat to equilibrate the pressure. The system then underwent equilibration with positional restraints on the solute: 25 ns with restraints on all solute atoms (Kr = 5 kcal mol^{-1} $Å^{-1}$), followed by 5 ns with restraints on Cα protein atoms alone (Kr = 5 kcal mol^{-1} $Å^{-1}$). All restraints were then removed for production runs. The CPPTRAJ module and the UCSF Chimera 1.17 program were used to perform MD analysis and draw the figures, respectively.

2.5. Alzheimer's Disease-like model induction

SAβ (5 μl) was slowly delivered through a 10 μl microsyringe (Hamilton) into the lateral ventricle following the coordinates AP = −0.5, ML = 1, DV = −2.3, according to Paxinos and Franklin atlas [43]. Sham mice received an intracerebroventricular (i.c.v.) injection the same volume of vehicle. After injection, the needle was left in place for an additional 5 min period to prevent reflux of the solution along the needle insertion track. The establishment of AD-like symptoms is observed starting from the 7th-day post-injection, as previously described [35]. The site of injection was verified by identifying the needle track at the time of dissection. A representative image is shown in the Suppl. Fig. 2.

2.6. Experimental design

To test the efficacy of PEA-OXA in limiting or counteracting sAβ-induced AD-like symptoms we used preventive or therapeutic pharmacological administration regimens. In the first experiment, the chronic administration (PEA-OXA 10 mg/kg *os* or vehicle) was undertaken after recovery from sAβ or saline 0.9 % i.c.v. injection. Behavioural, biochemical, and morphological analyses were carried out between the 7th-10th day post-surgery. Electrophysiological experiments were performed after behavioural analysis assuring cognitive impairment development (11th-14th day post-surgery). Treatment was continued until sacrifice. In different experimental groups, the acute therapeutic potential was assessed by a single i.p. administration 7 days post-surgery, followed by behavioural or electrophysiological evaluations 1 h and 24 h after treatment. Mice were casually randomized in four experimental groups for the preventive chronic treatment (Sham/veh, sham/PEA-OXA, saβ/veh, saβ/PEA-OXA), and six groups for the acute single injection (Sham/veh, sham/PEA-OXA 1 h, sham/PEA-OXA 24 h, saβ/veh, saβ/PEA-OXA 1 h, saβ/PEA-OXA 24 h). Each group was identified by an alphanumeric code and all experiments have been carried out by blind operators.

2.7. Cognitive performance evaluation

2.7.1. Novel object recognition test

The three stages of novel object recognition were habituation, familiarization, and testing. Habituation consisted of a free exploration of a polyvinyl chloride (PVC) box (40 × 30 × 30 cm), illuminated by a weak light, for 10 min. During the familiarization session, each mouse was allowed to explore two identical objects placed in the back corners of the box (left and right) for 5 min. In the trial test (conducted an hour or 24 h after the acquisition), one of the two objects was swapped out for a new, different object. The duration of time spent exploring the objects was recorded. Results were reported as recognition index (R.I.) calculated by the formula: exploration time of the novel object – exploration time of familiar object/ total exploration time [44]. In the acute therapeutic testing, the drug or vehicle was administered 15 min before the acquisition trial.

2.7.2. Y maze forced alternation test

The Y-maze forced alternation test protocol, was adapted from Wolf et al., with minimal variations. The apparatus consisted of three enclosed arms (30 × 5 × 15 cm) converging in the centre. To reduce anxiety, light in the testing area was dimmed to 30 ± 5 lux. The test consisted in a 5.min trial in which the mouse was allowed to explore only two arms of the Y-maze. Mice were returned to their cages during an inter-trial interval of 30 min. In the retrieval trial (5 min), the block of the third arm was removed. The latency to enter the novel arm, the time spent to explore it (%), and the number of entries in the first minute of the retrieval trial were recorded. Mice that entered the novel arm less than three times were excluded [45].

2.8. Social behaviour

2.8.1. Three chambers sociability test

The test consisted of a habituation period (5 min), followed by two consecutive sessions (10+10 min), testing sociability and social recognition memory, respectively. During the habituation, the mouse was allowed to freely explore the three chambers of the apparatus. Then, the mouse was brought into the centre chamber and temporarily held there. The following 10-minute sessions consists of placing an upside-down stainless-steel basket (6.5 × 15 cm) in one of the lateral chambers and an unfamiliar intruder in an identical upside-down cup in the opposite chamber. In the second session another intruder was introduced, exchanging the position of the first intruder. The time spent sniffing the basket or the intruders, and the number of entries into each lateral chamber were recorded [46].

2.9. In vivo electrophysiological recording

2.9.1. Long-term potentiation (LTP) in the LEC-DG pathway

Long Term Potentiation (LTP) was detected in the lateral entorhinal cortex-dentate gyrus (LEC-DG) pathway. Under urethane anaesthesia (1.5 g/kg i.p.) mice were fixed on a stereotaxic apparatus (Stoelting Co USA) to insert a stimulation electrode in the angular bundle of the lateral entorhinal cortex-LEC (AP: - 4.0 mm from bregma; ML: 4.5 mm from midline and DV: - 2.9 mm below the dura) and a recording electrode in the dentate gyrus-DG hilum (AP: - 2.1 mm from bregma, ML: 1.5 mm from midline and DV: - 1.2 mm below the dura mater), following Paxinos and Franklin atlas [43]. The stimulating and recording electrodes were slowly lowered in the mentioned areas until a field excitatory post-synaptic potential (fEPSP) appeared under low-frequency stimulation (0.033 Hz). A 30-min stable baseline was recorded, followed by the delivery to the LEC of tetanus (theta burst stimulation, TBS) consisting of 6 trains, 6 bursts, 6 pulses a 400 Hz, inter-burst interval: 200 ms, inter-train interval: 20 s [47]. Evoked responses after TBS, were recorded for 90–120 min. Long Term Potentiation (LTP) establishment was considered when the amplitude and the slope of fEPSPs increased more than 20 % for at least 30 min after the TBS, as previously reported [48]. The fEPSPs recorded before and after LTP were stored for analysis of slope and spike amplitude (WinLTP 2.30, Bristol, UK). In LTP experiments, all data points were normalized to the average baseline slope. The same protocol was applied for the preventive chronically treated dataset (daily vehicle or PEA-OXA 10 mg/kg *os*) and in acute challenge single administration of vehicle or PEA-OXA 10 mg/kg. In the latest dataset, the oral administration was technically limited by the

anaesthesia protocol that could influence the drug bioavailability, for this reason, we choose the i.p. route (1 h and 24 h before the LTP recording).

2.10. Biomolecular analysis

2.10.1. RNA extraction and semi-quantitative Real Time-PCR analysis

Hippocampal RNA extraction was obtained using the RDP Trio™ (HIMEDIA®) kit, according to the Chomczynski and Sacchi protocol [49]. Spectrophotometry (Nanodrop™) was used to test the RNA concentration by determining the absorbance values at a wavelength (λ) of 260 nm. The ratios A260/A280 and A260/A230 were detected to assess protein or organic solvent contaminations, respectively. The integrity and DNA genomic contamination was verified by electrophoresis. The reverse transcription was performed by using the 5X All-In-One RT Master Mix (abm®) according to the manufacturer's instructions. Semi-quantitative Real Time-PCR analyses were carried out on 100 ng DNA-free RNA, using the PrimePCR™ SYBR® Green Assay (Bio-Rad Laboratories ®). The reaction mixture volume was 10 μl and each primer (Table 1) was used at a final concentration of 300 nM. Each experimental set was run in triplicate using the BioRad CFX96 Real-Time PCR detection system (Bio-Rad Laboratories Inc.). Moreover, a non-reverse transcription control and a no template negative control were included. According to the manufacturer's instructions, the thermocycling protocol consisted of an activation cycle of 2 min at 95 °C followed by 40 cycles including a denaturation step (5 s at 95 °C), an annealing/extension step (30 s at 60 °C), and an extension step at 72 °C using SYBR green as detection system. Melt curve analysis confirmed that a single PCR product was present. Relative changes in gene expression were quantified using the comparative Ct (ΔCt, ΔΔCt) method, and Ct values were normalized to an average of the endogenous housekeeping gene Gapdh. mRNA expression of target genes was defined as fold change ($2^{\Delta\Delta Ct}$) in the expression level relative to the control group.

2.10.2. Western blot

Total proteins were extracted from the mice hippocampi resuspending tissues in RIPA buffer 1X and centrifugated at 12,000 rpm. Protein concentration was determined through the Bradford assay. A calibration curve was obtained using progressive Bovine Serum Albumin (BSA) dilutions of known concentrations. Using the standard curve, the concentration of each sample was determined according to its absorbance by interpolation. The absorbance was detected by using UV/VIS Spectrophotometer Jasco V-530. 50 μg of proteins were solubilized in 4X loading buffer, denaturized for 10 min at 95 °C, and separated on 8 or 10 % polyacrylamide SDS-gel performing SDS-PAGE electrophoresis at 10 V/cm. Then, the proteins were transferred to nitrocellulose membranes by using Trans-Blot Turbo Transfer System (Bio-Rad Laboratories, Hercules, CA, USA). After that, the membranes were blocked with TBST and 0.5 % non-fat milk for 1 h at RT to reduce unspecific binding. The membranes were further incubated with primary antibodies, solved in a solution of 5 % nonfat milk in TBST, overnight at 4 °C. Primary antibodies transglutaminase 2 (TG2) (®Zedira, cat. A033), GAPDH (®Elabscience, cat. E-AB-20032) were used, all diluted at 1:1000. Horseradish peroxidase (HRP)-conjugated goat anti-mouse (Cat. n. GxMu-003-DHRPX) and HRP-conjugated goat anti-rabbit (Cat. n. GtxRb-003-DHRPX) secondary antibodies were obtained from ImmunoReagents-Inc. Both secondary antibodies were used at a dilution of 1:5000. The protein bands were detected using enhanced chemiluminescence detection reagents ECL (Amersham Biosciences) and visualized on ChemiDoc XRS+ System (BIORAD). Band images were densitometrically analyzed by using ImageJ software, version 1.53c 26.

2.11. Morphological analysis

2.11.1. Tissue Preparation

Mice were deeply anesthetized and transcardially perfused with saline solution (Tris HCl 0.1 M/EDTA 10 mM) followed by 4 % paraformaldehyde (PFA) in 0.01 M phosphate-buffered saline (PBS, pH 7.4). Brains collected for immunohistochemistry (IHC) were post-fixed for 24 h in 4 % PFA, then soaked in 30 % sucrose phosphate-buffered saline, and frozen in chilled isopentane on dry ice.

2.11.2. Immunohistochemistry

Brain coronal slices (25 μm-thick) were obtained by sliding microtome (Leica Biosystems) and processed for IHC. The following primary antibodies were used: mouse antibodies against the glial fibrillary acidic protein (GFAP) (1:2500; Sigma-Aldrich, Milano, Italy); rabbit antibodies against ionized calcium-binding adaptor molecule 1 (Iba1) (1:400; Wako Chemicals, Richmond, VA, USA). Briefly, sections were blocked in blocking solution (10 % serum, in 0.01 M PBS/0.25 % Triton-X100) for 1 h at room temperature (RT).

Each primary antibody was diluted in the blocking solution and incubated with free-floating sections for 48 h at 4 °C. After being washed in cold PBS, slices were incubated with the appropriate biotinylated secondary antibody (Vector Labs Inc., Burlingame, CA, USA; 1:200) for 90 min at RT. Samples were then processed using the Vectastain avidin-biotin peroxidase kit (Vector Labs Inc., Burlingame, CA, USA) for 90 min at RT, washed in 0.05 M Tris-HCl and reacted with 3.3-diaminobenzidine tetrahydrochloride (DAB; Sigma, 0.5 mg/ML in Tris-HCl) and 0.01 % hydrogen peroxide. Sections were mounted on chrome alum–gelatin-coated slides, dehydrated and coverslipped. [50].

2.11.3. Cell count analysis

IHC-stained sections were imaged using a Zeiss Axioscope 2 optical microscope equipped with a high-resolution digital camera (C4742–95, Hamamatsu Photonics, Italia), at a magnification of 10x, in grayscale mode. Measurements of the morphometric parameters of astrocytes and microglia were made using the image-assisted analysis system (MCID 7.1; Res Imaging. Inc, Canada). The measurements of the GFAP and Iba1 markers were made in the hippocampal regions dentate gyrus (DG),

Table 1
Primers for mRNA transcripts.

Gene ID and reference sequence	Forward	Reverse
GAPDH NM_001289726.1	5′-GGGCATCTTGGGCTACACTGAGGACC-3′	5′- GGGGGCCGAGTTGGGATAGGG-3′
TG2 NM_009373.3	5′-ACTTCGACGTGTTTGCCCACAT-3′	5′-TTGATGTCCTCAGTGCCACACT-3′
IL6 NM_031168.2	5′-GATGGATGCTACCAAACTGGAT- 3′	5′-CCAGGTAGCTATGGTACTCCAGA-3′
iNOS NM_010927.4	5′-TGAGCTCATCTTTGCCACCA-3′	5′-ACAGTTCCGAGCGTCAAAGA-3′
TNF-α NM_013693.3	5'-ACTGAACTTCGGGGTGATCG-3'	5'-ACTGATGAGAGGGAGGCCAT-3'
IL-1β NM_008361.4	5′-TCGGACCCATATGAGCTGAAAG-3′	5′-CCACAGGTATTTTGTCGTTGCT-3′

Primers for GAPDH, TG2, IL-6, iNOS, TNF-α and IL-1β.

Cornu Ammonis 1 (CA1), and 3 (CA3) and expressed as cell count, using a selected region of interest (ROI). Data were exported, and their mean was converted to a frequency-distributed histogram. Data are expressed in mean ± SEM.

2.12. Statistical analysis

Data were represented as mean ± SEM. The Kolmogorov– Smirnov test was used to test the normal distribution of data. All behavioural, electrophysiological, morphological, and biomolecular data were analyzed using two-way ANOVA followed by Tukey's post hoc multi-comparison test. P values < 0.05 were considered statistically significant. Statistical analysis was performed using Prism/Graphpad 8.0 software. All raw data are available on Mendeley Data Repository with the following identifier DOI: 10.17632/jc7jncy5fv.1.

3. Results

3.1. Identification of the putative binding modes of PEA-OXA at rat α2AR by homology modeling, molecular docking, and molecular dynamics simulations

PEA-OXA was previously found to bind α2AR receptors with an IC_{50} of 0.75 μM in a ligand binding assay using rat cerebral cortical membranes and to act as an α2 antagonist in a low micromolar range [32]. α2AR include three highly homologous subtypes: α2A, α2B and α2C. Among these, the α2A subtype represents a promising target for AD, since its stimulation promotes Aβ generation and exacerbates AD-related pathology [51]. The lack of either any experimental data about receptor subtype selectivity or molecular insights into the binding mode for PEA-OXA prompted us to undertake a computational study focused on the α2A subtype, based on a molecular docking study followed by molecular dynamics (MD). The combination of docking and MD aims at a wider exploration of the conformational space accessible to the ligand within its binding site. This feature is particularly critical and challenging for PEA-OXA- α2AR complexes, because of the rather atypical chemical scaffold of PEA-OXA in comparison to canonical α2 ligands due to the absence of any positive charge and/or polar hydrogens, and to the elongated and highly flexible nature of the molecule. To better align computational with experimental data on binding, a homology model of the rat orthologue was built from the x-ray structure of the human α2A-adrenergic receptor, sharing > 90 % sequence identity, and used as the target in docking. Moreover, since rat and mouse α2A-adrenergic receptors share > 97 % of sequence identity, with most of the substitutions lying on the intracellular loop 3, far from the orthosteric binding site, no appreciable differences in the PEA-OXA binding are expected between the two orthologues. The representative binding poses from different docking runs (see the Methods section for details), collectively fit into a Y-shaped envelope in the binding site, as shown in Fig. 1A. The three arms of the "Y" correspond to the following binding subsites formed by polar residues interacting with the oxazoline ring: 1) $Tyr196^{5.38}$, $Ser200^{5.42}$ and $Tyr394^{6.55}$ (subsite 1), 2) $Ser90^{2.61}$, $Tyr109^{3.28}$, $Asp113^{3.32}$ and $Tyr416^{7.43}$ subsite 2) and 3) $Cys117^{3.36}$, $Trp387^{6.48}$, $Ser120^{3.39}$ (subsite 3). The latter subsite is located deep inside the helical bundle, close to the Na^{+} ion binding site. This site, formed by $Asp79^{2.50}$ and $Ser120^{3.39}$, is well-conserved within class A GPCRs and it is reported to negatively modulate the binding of agonists, without significantly affecting the binding of antagonists for α2AR [52–54]. The not-redundant representative docking poses from each binding site, namely pdock1, pdock2, and pdock3, underwent 100 ns of MD to assess their stability and to allow possible rearrangement/optimization from the starting docking poses. The complexes drifting toward dissociation during the first 100 ns were discarded from further analysis. The MD trajectories resulting in either substantially unchanged starting docking pose, or rearrangement into a new stable pose were further prolonged to ensure the lack of any (further) drift over a time scale of 200 ns. While the pdock3 pose was stable, providing a substantially unchanged MD-refined binding mode (hereinafter referred to as pMD3), a rearrangement was observed for pdock1 and pdock2. In particular, pdock1 moved toward the pdock3 binding site, giving rise to a new binding mode (hereinafter referred to as pMD1) with the oxazoline ring forming stable direct or water-mediated H-bonds with $Cys117^{3.36}$, $Trp387^{6.48}$, and $Ser120^{3.39}$ (see Fig. 1 B, panel a). pMD3, overlapping the same binding site, engages a stable stacking between the oxazoline ring and the $Trp387^{6.48}$ sidechain. Estimates of the electrostatic and van der Waals ligand-receptor interactions by a linear interaction energy (LIE) approach over the last 100 ns of trajectory show that pMD1 is energetically favored over pMD3 (−52.2 ± 2.6 vs −39.2 ± 2.0 kcal/mol) and was thus taken as representative for this binding site. pdock2 rearranged to an MD-refined binding mode (hereinafter referred to as pMD2) in which the ligand is H-bonded to $Trp387^{6.48}$ (direct) and $Asp113^{3.32}$ (water-mediated) as

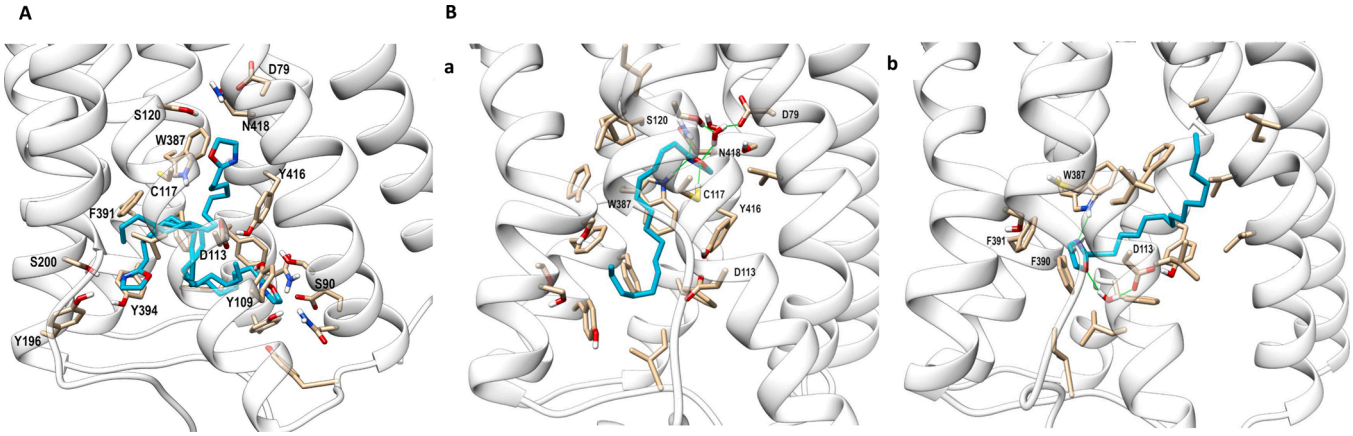

Fig. 1. Starting docking poses of PEA-OXA at α2A-adrenergic receptor and representative MD frames of the most stable complexes. A Representative docking poses from the three binding sites discussed in the main text. A stick representation is used for heavy atoms of the ligand (colored in cyan) and for protein sidechains (colored in tan while the ribbon is in white) within 5 Å of the ligand. Hydrogen, nitrogen, oxygen, and sulfur atoms are painted white, blue, red, and yellow, respectively. Half-transparency is employed for the ribbon representation of protein regions overlying the ligand in the selected view. **B** Representative MD frames of ligand pMD1 (panel a) and pMD2 (panel b). A stick representation is used for heavy atoms of the ligand (colored in cyan) and for protein sidechains (colored in tan while the ribbon is in white) within 5 Å of the ligand. Water molecules within 10 Å from the ligand involved in H-bonds are shown in stick representation. Hydrogen, nitrogen, oxygen, and sulfur atoms are painted white, blue, red, and yellow, respectively. Half-transparency is employed for the ribbon representation of protein regions overlying the ligand in the selected view. A green wire representation is adopted for H-bonds.

shown in Fig. 1B, panel b. The LIE value of pMD2 is comparable to that of pMD1 (−53.3 ± 2.3) vs − 52.2 ± 2.6 kcal/mol). The polar interaction with Asp113$^{3.32}$ is typical of a canonical α2 ligand. The oxazoline ring is also stabilized by hydrophobic interactions with the surrounding aromatic residues Phe390$^{6.51}$ and Phe391$^{6.52}$. The root-mean-square deviation (rmsd) values of pMD1 and pMD2 after the best fit of protein backbone over the last 200 ns of MD are shown in Suppl. Fig. 1A. The only rearrangement observed during this time scale is the conformation of the latter four (pMD1) or five (pMD2) carbon atoms of the alkyl chain. Finally, to get insight into possible PEA-OXA subtype selectivity, a comparative study at the level of protein sequences among the different subtypes including human, rat, and mouse orthologues was carried out and shown in Suppl. Fig. 1B. Since the residues forming either polar or hydrophobic interactions with PEA-OXA in the resulting poses are well conserved across the different subtypes, PEA-OXA can be considered a not-selective α2 antagonist.

3.2. Repeated administrations of PEA-OXA ameliorate cognitive performance and social behaviour in sAβ injected mice

The injection of sAβ induced cognitive impairments starting from the 7th-day post-injection. The daily treatment with PEA-OXA (10 mg/kg, *os*), undertaken on the same day of surgery, ameliorated the cognitive performance in sAβ mice. No difference was observed in PEA-OXA treated Sham mice. Schematic experimental plan is given in Fig. 2A.

The discriminative and spatial memory evaluation was carried out through Novel Object recognition and Y maze forced alternation test, respectively. In the Novel Object Recognition test, sAβ/veh mice showed a decreased recognition index (RI) compared to Sham/veh mice 1 h (RI: −0.02 ± 0.04 vs 0.26 ± 0.05, P = 0.033, $F_{model(1,28)}$ = 8.72) and 24 h (RI: 0.03 ± 0.09 vs 0.18 ± 0.01, P = 0.009, $F_{model(1,28)}$ = 4.07) after acquisition trial. The chronic treatment with PEAOXA normalized the RI in sAβ mice in both test trials, 1 h (RI= 0.22 ± 0.04 8 vs −0.02 ± 0.04, P = 0.01, $F_{treatment(1,28)}$ = 10.62, Fig. 2B) and 24 h (RI: 0.21 ± 0.09 vs 0.03 ± 0.09, $F_{treatment(1,28)}$ = 7.49, Fig. 2C).

In Y maze forced alternation test, a decrease in time spent in the novel arm was observed in sAβ/veh group compared to Sham/veh mice (26.23 ± 3.29 s vs 40.88 ± 2.27 s, P = 0.03, $F_{model(1,28)}$ = 18.09). The parameter was normalized in sAβ/PEA-OXA group compared to vehicle-treated mice (43.11 ± 2.42 s vs 26.23 ± 3.29 s, P = 0.038, $F_{treatment(1,28)}$ = 17.3), (Fig. 2D). Conversely, the latency to enter in the novel arm was increased in sAβ/veh mice compared to Sham/veh group (16.1.3 ± 2.17 vs 9 ± 1.69,P = 0.02, $F_{model(1,28)}$ = 9.12) and decreased by PEA-OXA chronic treatment (7.13 ± 1.61 vs 16.1.3 ± 2.17,P = 0.02, $F_{treatment(1,28)}$ = 9.58), (Fig. 2E).

In the three chambers sociability test, we obtained a significant increase in socialization with the mouse, instead of the object, in the sAβ/PEA-OXA group compared to vehicle-treated sAβ mice (interaction time: 51.38 ± 10.61 s vs 19.62 ± 2.56 s, P = 0.002, $F_{treatment(1,28)}$ = 11.35), suggesting a beneficial effect in overall social behaviour (Fig. 2F).

In addition, PEA-OXA treatment improved the social recognition memory, expressed as interaction time with the mouse II, resulted impaired in sAβ mice(interaction time: 38.00 ± 5.22 vs 16.5 ± 2.86 s, P = 0.03, $F_{treatment(1,28)}$ = 7.32), as compared to the controls (interaction time: 16.5 ± 2.86 s vs 45.63 ± 6.69 s, P = 0.002, $F_{model(1,28)}$ = 17.40), (Fig. 2G).

3.3. Repeated administrations of PEA-OXA partially revert the sAβ-induced LTP impairment in hippocampal DG

To investigate the impact of sAβ on hippocampal long-term synaptic plasticity, we analysed the LEC-DG pathway, schematically represented in Fig. 3A,B. As previously reported [55] sAβ-injected mice showed impaired LTP in DG granule cells compared to vehicle-treated animals, confirming that Aβ oligomers cause memory impairment. Since the preventive chronic treatment with PEA-OXA restored cognitive behaviour impairments in sAβ-injected mice, we investigated its effect on LTP at LEC-DG connectivity. To achieve this goal, we first assessed the

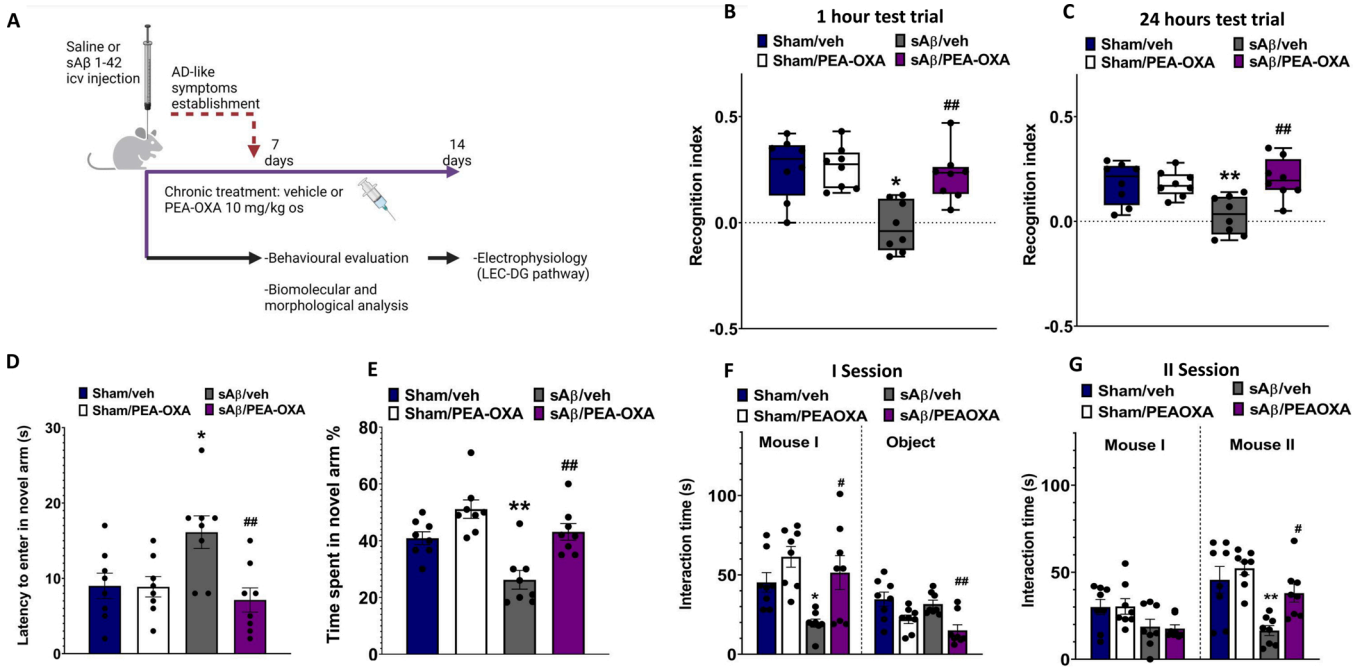

Fig. 2. Experimental plan, cognitive performance, and social behaviour A. Schematic timeline of the preventive treatment (veh or PEAOXA 10 mg/kg) experimental dataset. B, C show the recognition index (RI) of Novel Object Recognition test 1 h and 24 h after acquisition trial, respectively. D,E show the obtained in Forced Alternation Y-maze test. Specifically, latency to enter in the novel arm (seconds) and the % time spent in, respectively. E, F show the interaction time obtained in the I and the II session of Three Chambers Sociability test, respectively. All data are expressed as averaged mean ± SEM of 8 animals *per* group. Two-way ANOVA followed by Tukey's *post-hoc* test was used for analysis. P < 0.05 was considered statistically significant. Symbols: * indicates significant differences vs sham/veh; # indicates significant differences vs sAβ/veh.

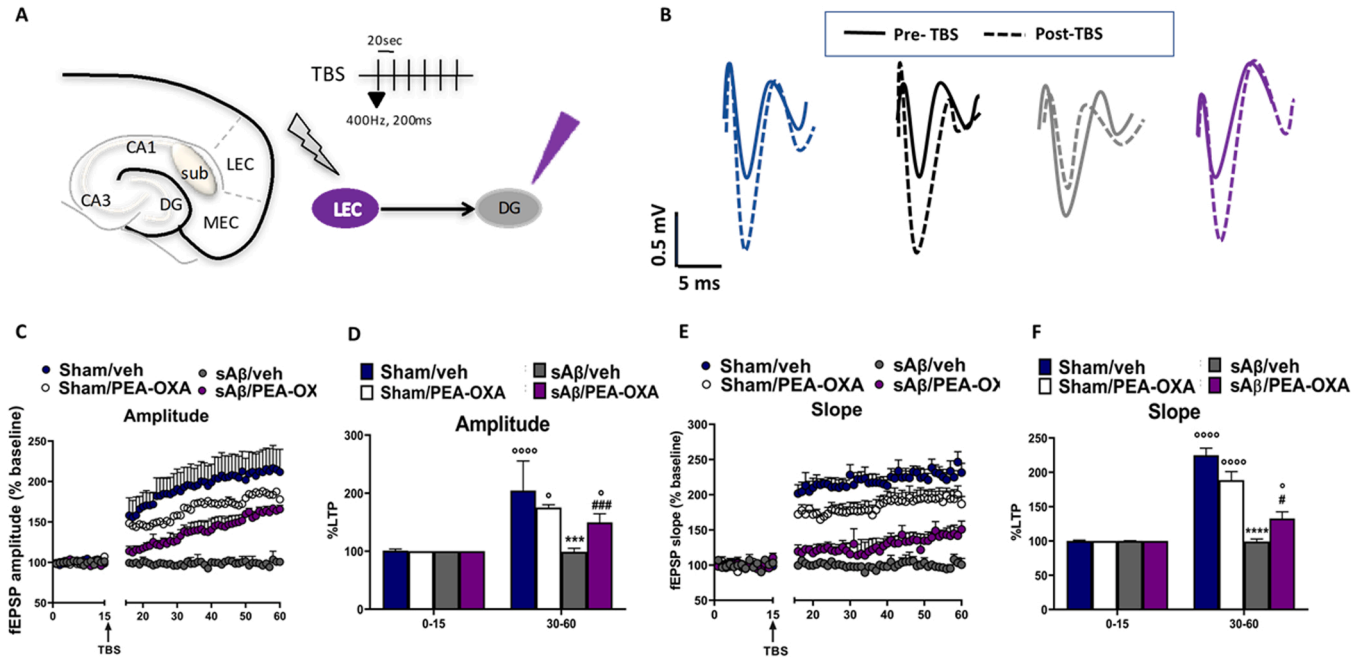

Fig. 3. In vivo recordings of long-term potentiation in LEC-DG pathway. A. Schematic representation of the position of the stimulating (lateral entorhinal cortex, LEC) and recording (dentate gyrus, DG) electrodes and the theta burst stimulation protocol (TBS) to evoke LTP in DG, consisted of 6 trains, 6 bursts, 6 pulses at 400 Hz, interburst interval: 200 ms, intertrain interval: 20 s B. Representative traces of a single evoked field excitatory postsynaptic potentials (fEPSP) recorded in DG before and after TBS protocol (black arrow) C. Shows the time-dependent changes in the fEPSP amplitude after TBS protocol application. Data plotted as % amplitude from baseline (0–15 min). D. Bar histogram of amplitude data averaged 30–60 min after TBS and normalized respect to the baseline (mean ± SEM). Data were analyzed by Two-way ANOVA followed by Tukey's *post-hoc* multicomparisons test, $P < 0.05$ was considered statistically significant. °indicates significant differences vs baseline (0–15 min); * indicates significant differences vs Sham/veh; # indicates significant differences vs sAβ/veh. E. Data points represent averaged slope (mean ± SEM) after TBS induction, normalized with respect to baseline values (0–15). F. Bar histogram of slope data averaged 30–60 min after TBS and normalized respect to the baseline (mean ± SEM). Data were analyzed by Two-way ANOVA followed by Tukey's *post-hoc* multicomparisons test, $P < 0.05$ was considered statistically significant. °indicates significant differences vs baseline (0–15 min); * indicates significant differences vs Sham/veh; # indicates significant differences vs sAβ/veh.

potential long-lasting modifications at synaptic strength in LEC-DG pathway in sAβ-injected mice treated with vehicle. As expected, LTP evoked at DG area of sham animals induced a significant increase of amplitude (30–60 min: 204.507 ± 25.5 %, vs 0–15 min: 100.96 ± 1.37 %, $P < 0.0001$; $F_{time(1,24)}$:171.6) and slope values (224.89 ± 10.20 % vs 0–15 min: 99.96 ± 1.10 %, $P < 0.0001$; $F_{time(1,24)}$:305), (Fig. 3C–F). Accordingly with behavioural observations, a theta burst stimulation in LEC failed to alter fEPSP amplitude (30–60 min: 98.85 ± 3.04 % vs 0–15 min: 100 %; $P > 0.99$) and slope (99.26 ± 3.58 % vs 100.167 ± 0.67 %; $P > 0.99$), (Fig. 3C–F). Remarkable, the preventive chronic treatment with PEA-OXA, induced a significant increase of synaptic efficiency after the LTP induction in term of amplitude (30–60 min: 149.62 ± 7.42 %, vs 0–15 min: 100 %, $P = 0.021$; Fig. 3C,D) and slope (132.71 ± 9.74 %, vs 0–15 min: 100 %, $P < 0.0001$; Fig. 3 E,F). Finally, no significant changes were observed in sham/PEA-OXA mice, neither in fEPSP amplitude (30–60 min: 190.12 ± 13.77 %, vs 0–15 min: 97.72 ± 2.69 %, $P = 0.021$; Fig. 2C,D) nor in slope (30–60 min: 206.53 ± 11.53 %, vs 0–15 min: 100.48 ± 1.58 %, $P < 0.0001$; Fig. 3C,D) after LEC TBS application (Fig. 3C–F).

3.4. Repeated administrations of PEA-OXA reduce microglial recruitment and morphological changes in sAβ-injected mice

We analyzed glial reactivity employing morphological markers for astrocytes and microglia in different hippocampal regions, namely dentate gyrus (DG), Cornu Ammonis (CA) 1, and 3.

Microglial Iba1 staining showed an increased cell count in sAβ/vehicle group compared to sham/veh mice in CA3 (69,79 ± 6,9 vs 41,39 ± 7,04, $P = 0.007$, $F_{model(1,8)} = 9.51$), as shown in Fig. 4. The treatment with PEA-OXA drastically reduced microglial density as compared to the vehicle (38,00 ± 2,821 vs 69,79 ± 6,9; $P = 0.03$, $F_{tratment(1,8)} = 12.79$). Fig. 4 also suggests that the microglia morphology is affected by PEA-OXA treatment by shifting the ameboid inflammatory phenotype (sAβ/veh), toward the star-shaped appearance (sAβ/PEA-OXA).

$GFAP^+$ astrocytes count suggested an increasing trend in the sAβ/PEA-OXA group compared to sham/veh mice in both CA1 (286,5 ± 44,77 vs 163,7 ± 42,51) and CA3 (148,0 ± 28,29 vs 84,80 ± 21,74), however without reaching significance (CA1: $P = 0.33$; CA3: $P = 0.27$) (Fig. 5).

Taken together these data about glial reactivity showed conclusive evidence of microglial precocious activation following intraventricular sAβ injection that was more evident in hippocampal CA3 and prevented by PEA-OXA repeated administrations. The changes were consistent in both cell count and morphological appearance.

3.5. Repeated administrations of PEA-OXA exert neuroprotective action against hippocampal damage induced by the injection of sAβ

3.5.1. sAβ – induced neuroinflammatory cytokines expression decreases in sAβ injected mice chronically treated with PEA-OXA

To evaluate inflammatory state, hippocampal cytokines mRNA levels were measured by Real Time PCR, as shown in Fig. 6A. 7 days post-sAβ (1−42)-injection, sAβ/veh group showed higher levels of pro-inflammatory cytokines compared to Sham/veh control group, specifically IL-6 (52.06 ± 0.79 vs 1, $P < 0.0001$, $F_{model(1,8)} = 1220$), iNOS (88.26 ± 1.45 vs 1, $P < 0.0001$, $F_{model(1,8)} = 1855$), TNF-α (24.31 ± 0.47 vs 1, $P < 0.0001$, $F_{model(1,8)} = 116.8$) and IL-1β(32.16 ± 1.99 vs 1, $P < 0.0001$, $F_{model(1,8)} = 145.9$). Chronic PEA-OXA treatment down-regulated cytokines mRNA levels in sAβ mice [IL6: 6.4 ± 1.03 vs

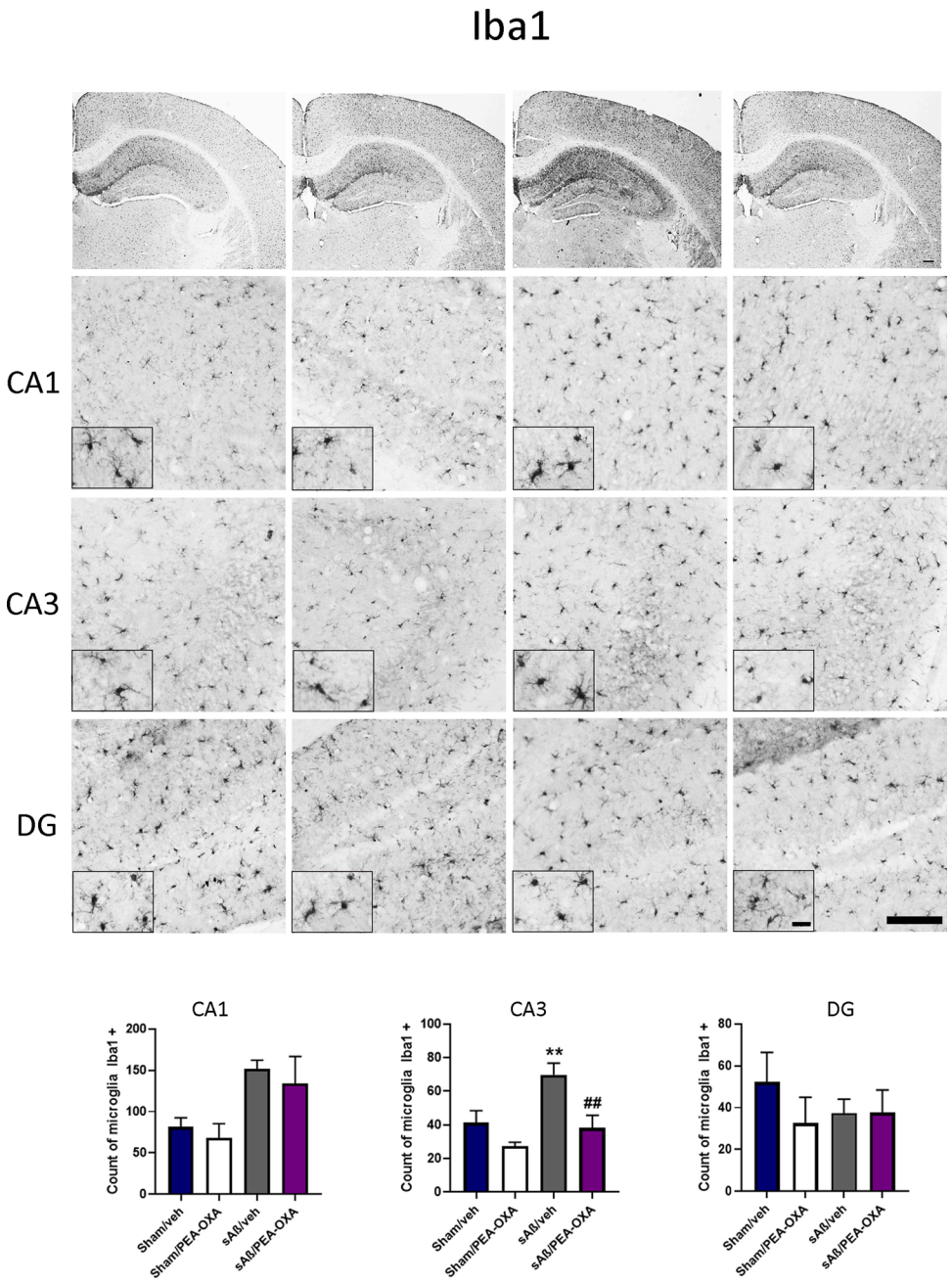

Fig. 4. Microglia evaluation in the Hippocampus. Comparison of region-specific microglial response in the hippocampus. All hippocampus coronal sections (2.5x) DG, CA1, and CA3 (20x) regional expressions of Iba1 for the different groups are showed. Small boxes (40x) for each region are represented to visualize cellular morphology. Scale bars 50 μm. Data of cell count are expressed on the graph as mean ± SEM. Two-way ANOVA followed by Tukey's post hoc test was used for multicomparisons analysis. (* indicates significant differences vs sham/veh; # indicates significant differences vs sAβ/veh).

52.06 ± 0.79, P < 0.0001, $F_{treatment(1,8)}$ = 782.21; iNOS: 2.17 ± 1.86 vs 88.26 ± 1.45, P < 0.0001, $F_{treatment(1,8)}$ = 1756; TNF-α: 3.99 ± 1.37 vs 24.31 ± 0.47, P < 0.0001, $F_{treatment(1,8)}$ = 62.18; IL-1β: 4.11 ± 1.22 vs 32.16 ± 1.99, P < 0.0001, $F_{treatment(1,8)}$ = 94.02]. No significant difference was reported in Sham/PEA-OXA treated mice compared to Sham/veh group.

3.5.2. *PEA-OXA chronic treatment down-regulates sAβ – induced Transglutaminase 2 expression in sAβ injected mice*

As a marker of inflammation the Transglutaminase 2 (TG2) mRNA and protein levels were determined by Real-Time PCR and Western Blot, respectively, in the hippocampus, as shown in Fig. 6B,C. Compared to control group, TG2 was up-regulated in sAβ/veh mice in both mRNA quote (3.69 ± 0.66 vs 1, P = 0.007, $F_{model(1,8)}$ = 16.07) and protein relative expression (153.67 ± 2.4 vs 100, P < 0.0001, $F_{model(1,8)}$ = 373.1). Chronic PEA-OXA treated sAβ mice showed reduced TG2levels, in both mRNA (1.97 ± 0.41 vs 3.69 ± 0.66, P = 0.017, $F_{treatment(1,8)}$ = 2.53) and protein (39.67 ± 2.4 vs 153.67 ± 2.4, P < 0.0001, $F_{model(1,8)}$ = 569.3). No significant changes were found between Sham/veh and sham PEA-OXA groups. Full-length gels are shown in the Suppl. Fig. 3.

3.6. *Single administration of PEA-OXA reduces cognitive impairments and reverts the sAβ-induced LTP impairment in hippocampal DG*

To test the therapeutic potential of PEA-OXA when memory alterations were established, we tested the effect of a single administration in both behavioural and electrophysiological tasks. We found that PEA-OXA (10 mg/kg i.p.) was able to normalize the impaired R.I. in NOR 1 h test trial, as compared to vehicle in sAβ group (0.25 ± 0.11 vs −0.04 ± 0.09, P = 0.0003, $F_{treatment(1,28)}$ = 10.23), observing a wearing off effect in the NOR 24 h trial (−0.02 ± 0.07 vs −0.004 ± 0.05). Results are shown in the Suppl. Fig. 4. No difference was observed in sham/PEA-OXA mice compared to control group. Accordingly, administering PEA-OXA 1 h before LTP recording, we found a significant enhancement of

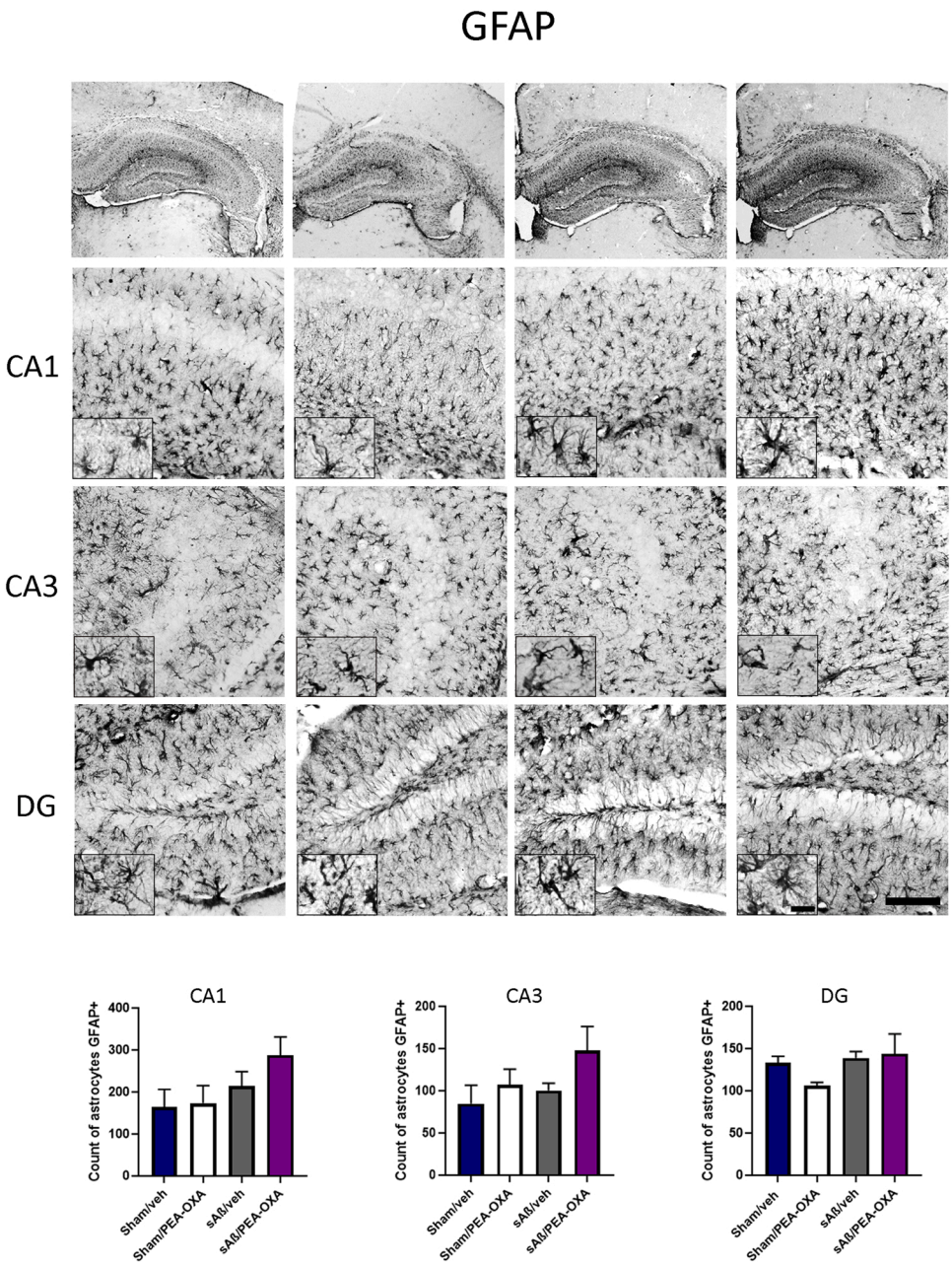

Fig. 5. Astrocytes evaluation in the Hippocampus. Comparison of region-specific astrocytic response in the hippocampus. All hippocampus coronal sections (2.5x) DG, CA1, and CA3 (20x) regional expressions of GFAP for the different groups are demonstrated. Small boxes (40x) for each region are represented to visualize cellular morphology. Scale bars 50 μm. Data of cell count are expressed on the graph as mean ± SEM. Two-way ANOVA for repeated measures followed by Tukey's post hoc test was used for multicomparisons analysis. (* indicates significant differences vs Sham/veh; # indicates significant differences vs sAβ/veh).

LTP in sAβ animals as compared to vehicle-injected mice (fEPSP amplitude 30–60 min: 138.99 ± 4.6 vs 98.34 ± 2, P = 0.004, $F_{treatment\ (5,32)} = 21.33$; fEPSP slope 30–60 min: 149.64 ± 5.16 vs 99.26 ± 3.58, P = 0.0007, $F_{treatment(5,32)} = 23.75$), as shown in Suppl. Fig. 4. On the contrary, the same treatment 24 h prior LTP induction did not affect LTP in sAβ-injected mice (fEPSP amplitude 30–60 min: 102.26 ± 8.26; fEPSP slope 30–60 min: 104.91 ± 4.92). Sham mice subjected to PEA-OXA acute treatment, showed modifications neither in basal synaptic properties including input-output (I-O) relationship nor in LTP magnitude.

4. Discussion

The objective of this study was to investigate the effect of the natural α2AR modulating compound PEA-OXA in limiting the cognitive deficits associated with the sAβ-induced AD-like model. This stems from the growing interest in the role of these receptors in several progressive neurodegenerative diseases [56–59]. In this study, we highlighted the effects of PEA-OXA, a natural molecule that we previously found to bind α2 and H3 receptors [31,32], in dementia-like behaviours induced by the sAβ.

First, we focused our interest on PEA-OXA capability to act as an α2A-adrenergic antagonist, investigating in silico its ability to bind this subtype, a relevant pharmacological target in AD. Indeed, a computational approach combining molecular docking and molecular dynamics led to the identification of two spatially-close putative binding sites for PEA-OXA on the α2A-adrenergic receptor. In both poses, namely pMD1 and pMD2, the oxazoline ring is involved in H-bonds with $Trp387^{6.48}$, although the molecule features two distinct orientations, tilted by 90°: in pMD1 it lies parallel to the helix bundle, accommodating the oxazoline ring in a narrow binding pocket close to the Na^+ binding site, while in pMD2 it spans the orthosteric binding site perpendicularly to the helix bundle. In pMD1, the oxazoline ring forms a network of either direct or water-mediated H-bonds, in addition to those with $Trp387^{6.48}$,

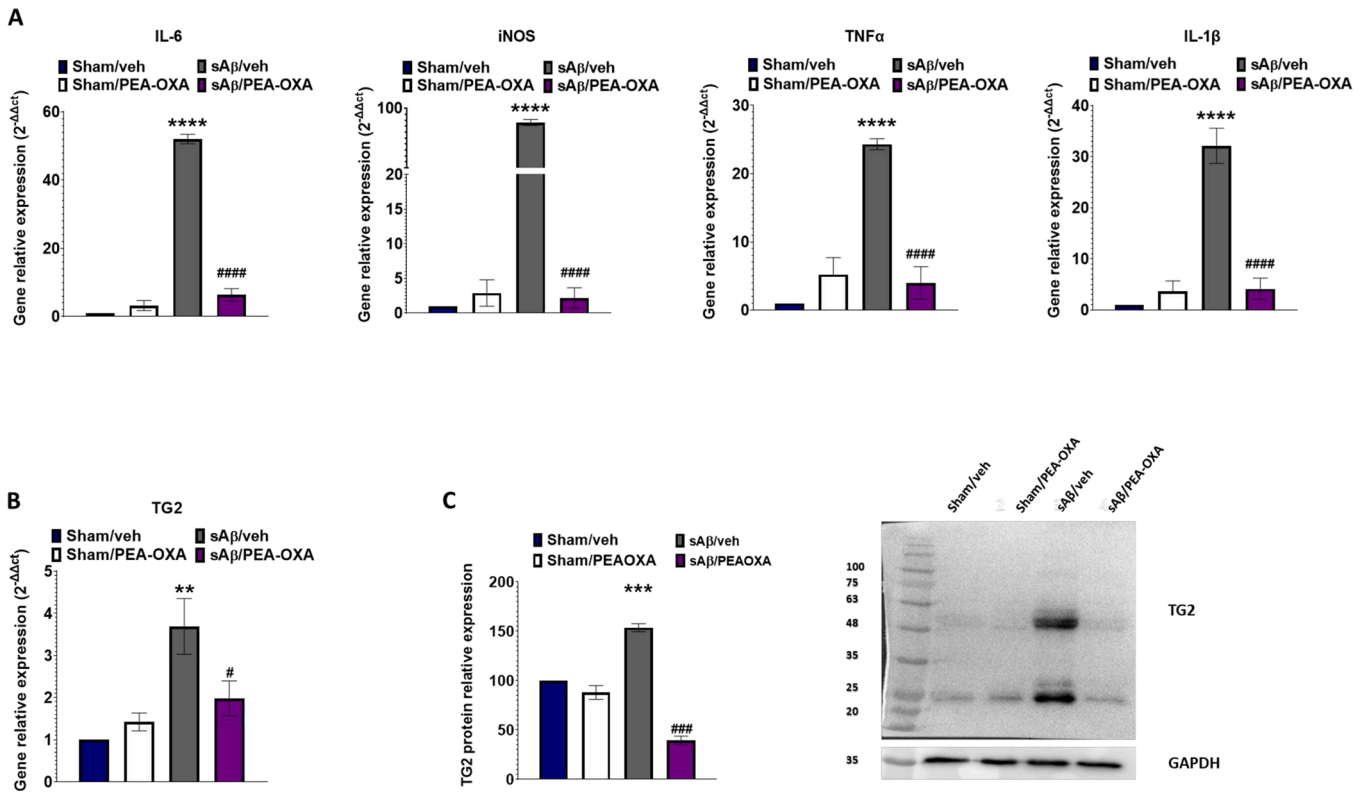

Fig. 6. Hippocampal pro-inflammatory cytokine panel and TG2 evaluation. A. Relative mRNA expression of hippocampus neuroinflammatory cytokines detected by Real Time PCR. GAPDH was used as housekeeping gene to normalize. Data are shown as the mean ± SEM of three independent experiments. Two-way ANOVA for repeated measures followed by Tukey's post hoc test was used for multicomparisons analysis. (* indicates significant differences vs sham/veh; # indicates significant differences vs sAβ/veh). B. Hippocampus Transglutaminase 2 (TG2) mRNA analyzed by Real Time PCR. C. Protein relative expression of hippocampal TG2 obtained by Western Blot. Data are shown as the mean ± SEM of three independent experiments, normalized respect to GAPDH, as housekeeping gene. Two-way ANOVA for repeated measures followed by Tukey's post hoc test was used for multicomparisons analysis. (* indicates significant differences vs Sham/veh; # indicates significant differences vs sAβ/veh).

Cys117$^{3.36}$, Ser120$^{3.39}$, and Asn418$^{7.45}$, while the alkyl chain forms hydrophobic interactions with the residues facing the orthosteric ligand binding site. Instead, in pMD2, the oxazoline ring forms hydrophobic interactions with the aromatic residues Phe390$^{6.51}$ and Phe391$^{6.52}$ and engages a water-mediated H-bond with Asp113, a residue usually involved in H-bonds reinforced by ionic interactions with canonical α2-adrenergic ligands. In pMD2, the hydrophobic interactions of the ligand alkyl chain extend outside the ligand-binding site, to residues lying at the interface between helices H2 and H3. Both poses identified in this study differ from the classical orientation of canonical ligands, (e.g., catecholamines, imidazolines, and azepines). Most of these molecules have rigid aromatic scaffolds, polar hydrogens, and positive charges, which typically form a network of polar interactions involving Asp113$^{3.32}$, Tyr416$^{7.43}$, Ser200$^{5.42}$, and Tyr394^{6,55}. In this view, PEA-OXA represents a novel and atypical class of α2-adrenergic modulators due to either its elongated and flexible nature and the absence of any positive charge/polar hydrogens. As observed in both docking and MD studies, PEA-OXA, thanks to its negligible steric hindrance and pure H-bond acceptor oxazoline ring, can reach a deeper binding site not reported before for other α2 adrenergic ligands, located within the helix bundle in spatial proximity to the Na^+ binding site, a well-known negative modulator for this class of receptors.

Considering such a unique interaction of PEA-OXA with α2 adrenoceptors, this is a molecule that, on one side, adds complexity to the mechanism of action, on the other side, has unique characteristics that give it further value. We have previously shown that PEA-OXA prevents social interaction impairments, aggressiveness, and depression in a traumatic brain injury model [32]. Since PEA-OXA was effective in ameliorating a wide range of symptoms including the recovery of spatial memory from mTBI, we investigated this molecule in other neuropsychiatric conditions of different origins. This idea comes also from the evidence that both GABAergic and dopaminergic neurotransmission are improved in the mPFC after treatment with PEA-OXA, together with the normalization of neuronal activity [32]. Indeed, the crucial role of these two neurotransmissions in the genesis of various disorders in the neuropsychiatric field, from depression to psychosis and dementias, has been largely described [60–63].

PEA-OXA allowed the normal hippocampal neuroplasticity (recovery of the LTP in the DG) and the dopamine, norepinephrine, histamine, glutamate, and GABA released in the DG of the hippocampus of spared nerve injury (SNI) neuropathic mice. At the same time, it counteracted both depressive-like behaviors and cognitive impairment due to SNI [31]. More recently, PEA-OXA has also been shown to be effective in reducing behavioral disturbances associated with persistent stress from chronic social isolation in mice [64].

Noradrenergic neurons of the LC are among the first in the CNS to die at the onset of AD [56,65–67]. It is accepted that the agitation, aggressive behaviour, and sleep disturbances of AD [56,66,68] are connected to a maladaptive LC cell modulation aimed at compensating for the norepinephrine deficiency [68–70]. Therefore, the LC has been considered an important target for the pathophysiology of dementias and AD in the last years [71–74]. More recent evidence would even demonstrate the direct link between Aβ and α2AR. This direct allosteric interaction may lead to a sort of hijacking of the receptor towards the exclusive activation of a post-receptor pathway driving the over-activation of glycogen-synthase-3 kinase beta (GSK3). This kinase is responsible for tau over-phosphorylation [75,76] and could have a good relationship with the pathogenesis of both sporadic and familial

forms of AD [77–79]. In this contest, another aspect to be considered is the high expression of α2AR adrenoceptors in noradrenergic neurons, this makes LC neurons selectively vulnerable if assembly and activation of the Aβ/α2 receptor complexes occur. The α2AR upregulation in AD or other types of dementias has been shown also in the human brain [80].

The pharmacological block of the α2AR, causing an extracellular increase of norepinephrine, allows a greater activation of the β and α1AR, which are involved in neuroplasticity and neurotrophic actions. So much so that one of the possible adverse reactions of β-blockers or even some α1 antagonists (i.e tamsulosin) is depression, if not a suspected increased risk of hypo-cognition [81,82]. Finally, the anti-inflammatory activity recognized of catecholamines in the CNS, in particular noradrenaline, in reducing the release of pro-inflammatory cytokines and facilitating the synthesis of IL4 or IL10 should be taken into consideration [15,83–85]. Indeed, we reported that PEA-OXA normalized the levels of some cytokines or neuro-inflammatory and pro-apoptotic factors (i.e TG2) in the hippocampus that were upregulated by Aβ exposure (see below). Collectively, these considerations are strongly in line with the results obtained in this study. In fact, in a prophylactic regimen, PEA-OXA counteracted the cognitive damage, in terms of spatial and discriminatory memory. Moreover, it improved the social behaviour and retrieved the social recognition memory impairment induced by Aβ. Consistently, this was accompanied by a normalizing effect of neuronal plasticity within the LEC-DG pathway (i.e. LTP), which is directly involved in memory and learning [44,86]. Moreover, it is interesting to note that long-term treatment was needed to induce lasting synaptic restoration with PEA-OXA. A single PEA-OXA challenge exerted a transient effect by improving the recognition index and neuronal plasticity. These ameliorative effects were perhaps due to a fleeting action on the noradrenergic system without exerting a lasting effect to ensure long-term synaptic remodelling and plasticity. Furthermore, PEA-OXA reduced the expression of involved genes in neuroinflammation. The analysis, carried out by ELISA on the dissected DG of the hippocampus, showed a reduction in the transcripts of IL1b, IL6, TNFa, and iNOS.

Another important specific neurodegenerative diseases target [87,88] and neuroinflammation marker [89], TG2 was also downregulated in CA3 as a translated product. There is evidence that the calcium-dependent transamidation activity of TG2 plays a critical role in the formation of neurotoxic protein aggregates such as toxic and insoluble amyloid proteins that participate in the pathogenesis of various neurodegenerative diseases [90]. So far, many important and neurodegeneration-related TG2 substrates have been identified, including mutant huntingtin, α-synuclein and Aβ, tau. Therefore, the fact that PEA-OXA downregulated the TG2 (although very likely with indirect mechanisms) places this molecule in a position with an added value to its anti-neuroinflammatory capabilities. This deserves consideration because the neo-formation of toxic peptides was inhibited by selective inhibitors of TG2 [91]. Therefore, being able to intervene with a natural molecule such as PEA-OXA could be a great opportunity to modulate the TG2-mediated proapoptotic pathways, as well as the molecular regulation systems underlying the progression of many progressive neurodegenerative disorders [92].

Behavioural and morpho-functional effects mediated by PEA-OXA were associated with the normalization of microglial density in the CA1 and CA3.

The function of microglia in AD pathophysiology has been described as ambivalent [93,94]. On one hand, microglia release inflammatory mediators triggered by Aβ production and accumulation. On the other hand, microglial activation is critical in its physiological clearance [93]. In this context, uncontrolled activation as well as loss of microglial function can lead to a disease-promoting environment. Different morphologies (hypertrophic and dystrophic microglia) have been found to play a role in brain aging and neuronal degeneration in AD, other types of dementia [95], and different cognitive deficits [96]. Even though we did not deeply analyse the microglial phenotypes in this study, the biomolecular changes observed at the same hippocampal level and microglial morphology allow us to assume that the increased microglial cells expressed a pro-inflammatory phenotype. Moreover, astrocytes demonstrated a non-significant involvement in the reactive gliosis phenomena of this model, confirming the different tuning of glial cells in maladaptive plasticity and neurodegeneration [97,98]. The relative quiescence of astrocytes in early neuroinflammatory changes of AD-like phenotype, further validates the pivotal role of microglia. The reduction of the neuroinflammatory processes induced by PEA-OXA in the CA1 CA3 hippocampus could be also involved, at least in part, in its capability in restoring the plastic changes at the electrophysiological level. Indeed, it is known that CA1 and CA3 receive input from the DG in which we performed LTP analysis.

5. Conclusions

In conclusion our findings indicate that PEA-OXA prevents the sAβ-induced cognitive damage in mice, by restoring synaptic plasticity and reducing neuroinflammation at hippocampal level. Moreover, we suggest that the intimate interaction of PEA-OXA with the α2AR could be correlated, at least in part, with these protective effects. Even though the noradrenergic "dysfunction" cannot be the only one responsible for the complex dimensions that characterize AD, it may be worth studying the pro-cognitive potential of the α2AR antagonists and therefore re-proposing their clinical tests in some forms of dementias.

On these bases, PEA-OXA may be considered as a novel compound for future innovative approaches to dementia or AD for which the available drugs are poorly effective. However, further preclinical studies, employing α2AR ligands in putative translationally relevant models of neuropsychiatric illness, will be critical to validate α2-AR as pharmacological target in AD-like diseases.

CRediT authorship contribution statement

R. Infantino: Conceptualization, Data curation, Investigation. **S. Boccella:** Data curation, Investigation. **F. Ricciardi:** Investigation. **D. Scuteri:** Data curation. **M. Perrone:** Investigation. **R.M. Vitale:** Investigation, Methodology. **R. Bonsale:** Investigation. **A. Parente:** Investigation, Methodology. **I. Allocca:** Investigation. A. Virtuoso: Investigation, Methodology. **C. De Luca:** Investigation, Methodology. **C. Belardo:** Investigation, Methodology. **P. Amodeo:** Investigation. **V. Gentile:** Project administration. **G. Cirillo:** Project administration. **G. Bagetta:** Conceptualization, Project administration, Writing - original draft. **L. Luongo:** Conceptualization, Funding acquisition, Writing - review & editing. **S. Maione:** Conceptualization, Funding acquisition, Writing - original draft. **F. Guida:** Conceptualization, Project administration, Writing - review & editing.

Conflict of interest statement

The Authors declare that there is no conflict of interest.

Appendix A. Supporting information

Supplementary data associated with this article can be found in the online version at doi:10.1016/j.biopha.2022.113844.

References

[1] M.V.F. Silva, C. de, M.G. Loures, L.C.V. Alves, L.C. de Souza, K.B.G. Borges, M. das, G. Carvalho, Alzheimer's disease: risk factors and potentially protective measures, J. Biomed. Sci. 26 (2019) 33, https://doi.org/10.1186/s12929-019-0524-y.

[2] C. Ballard, S. Gauthier, A. Corbett, C. Brayne, D. Aarsland, E. Jones, Alzheimer's disease, Lancet 377 (2011) 1019–1031, https://doi.org/10.1016/S0140-6736(10)61349-9.

[3] A. Wimo, L. Jönsson, J. Bond, M. Prince, B. Winblad, The worldwide economic impact of dementia 2010, Alzheimers Dement. 9 (2013) 1–11.e3, https://doi.org/10.1016/j.jalz.2012.11.006.

[4] P. Scheltens, B. De Strooper, M. Kivipelto, H. Holstege, G. Chételat, C.E. Teunissen, J. Cummings, W.M. van der Flier, Alzheimer's disease, Lancet 397 (2021) 1577–1590, https://doi.org/10.1016/S0140-6736(20)32205-4.

[5] H. Hampel, J. Hardy, K. Blennow, C. Chen, G. Perry, S.H. Kim, V.L. Villemagne, P. Aisen, M. Vendruscolo, T. Iwatsubo, C.L. Masters, M. Cho, L. Lannfelt, J. L. Cummings, A. Vergallo, The amyloid-β pathway in alzheimer's disease, Mol. Psychiatry 26 (2021) 5481–5503, https://doi.org/10.1038/s41380-021-01249-0.

[6] M.A. Busche, B.T. Hyman, Synergy between amyloid-β and tau in Alzheimer's disease, Nat. Neurosci. 23 (2020) 1183–1193, https://doi.org/10.1038/s41593-020-0687-6.

[7] T.L. Spires-Jones, B.T. Hyman, The intersection of amyloid beta and tau at synapses in Alzheimer's disease, Neuron 82 (2014) 756–771, https://doi.org/10.1016/j.neuron.2014.05.004.

[8] S. Ludewig, M. Korte, Novel Insights into the physiological function of the APP (Gene) family and its proteolytic fragments in synaptic plasticity, Front. Mol. Neurosci. 9 (2016) 161, https://doi.org/10.3389/fnmol.2016.00161.

[9] Y. Mu, F.H. Gage, Adult hippocampal neurogenesis and its role in Alzheimer's disease, Mol. Neurodegener. 6 (2011) 85, https://doi.org/10.1186/1750-1326-6-85.

[10] K.R. Babcock, J.S. Page, J.R. Fallon, A.E. Webb, Adult hippocampal neurogenesis in aging and Alzheimer's Disease, Stem Cell Rep. 16 (2021) 681–693, https://doi.org/10.1016/j.stemcr.2021.01.019.

[11] G.-F. Chen, T.-H. Xu, Y. Yan, Y.-R. Zhou, Y. Jiang, K. Melcher, H.E. Xu, Amyloid beta: structure, biology and structure-based therapeutic development, Acta Pharmacol. Sin. 38 (2017) 1205–1235, https://doi.org/10.1038/aps.2017.28.

[12] M.S. Uddin, M.T. Kabir, M.S. Rahman, T. Behl, P. Jeandet, G.M. Ashraf, A. Najda, M.N. Bin-Jumah, H.R. El-Seedi, M.M. Abdel-Daim, Revisiting the amyloid cascade hypothesis: from anti-Aβ therapeutics to auspicious new ways for alzheimer's disease, Int. J. Mol. Sci. 21 (2020), https://doi.org/10.3390/ijms21165858.

[13] P. Juhl-Olsen, C.A. Frederiksen, E. Sloth, Ultrasound assessment of inferior vena cava collapsibility is not a valid measure of preload changes during triggered positive pressure ventilation: a controlled cross-over study, Ultraschall Der Med. 33 (2012) 152–159, https://doi.org/10.1055/s-0031-1281832.

[14] H. Hampel, M.-M. Mesulam, A.C. Cuello, A.S. Khachaturian, A. Vergallo, M. R. Farlow, P.J. Snyder, E. Giacobini, Z.S. Khachaturian, Revisiting the cholinergic hypothesis in alzheimer's disease: emerging evidence from translational and clinical research, J. Prev. Alzheimer's Dis. 6 (2019) 2–15, https://doi.org/10.14283/jpad.2018.43.

[15] G. Leanza, R. Gulino, R. Zorec, Noradrenergic hypothesis linking neurodegeneration-based cognitive decline and astroglia, Front. Mol. Neurosci. 11 (2018) 254, https://doi.org/10.3389/fnmol.2018.00254.

[16] A. Zlomuzica, D. Dere, S. Binder, M.A. De Souza Silva, J.P. Huston, E. Dere, Neuronal histamine and cognitive symptoms in Alzheimer's disease, Neuropharmacology 106 (2016) 135–145, https://doi.org/10.1016/j.neuropharm.2015.05.007.

[17] H.C. Dringenberg, Alzheimer's disease: more than a "cholinergic disorder" - evidence that cholinergic-monoaminergic interactions contribute to EEG slowing and dementia, Behav. Brain Res. 115 (2000) 235–249, https://doi.org/10.1016/s0166-4328(00)00261-8.

[18] V. Haroutunian, A.C. Santucci, K.L. Davis, Implications of multiple transmitter system lesions for cholinomimetic therapy in Alzheimer's disease, Prog. Brain Res. 84 (1990) 333–346, https://doi.org/10.1016/s0079-6123(08)60917-6.

[19] J.F. Smiley, M. Subramanian, M.M. Mesulam, Monoaminergic-cholinergic interactions in the primate basal forebrain, Neuroscience 93 (1999) 817–829, https://doi.org/10.1016/s0306-4522(99)00116-5.

[20] L. Záborszky, W.E. Cullinan, V.N. Luine, Catecholaminergic-cholinergic interaction in the basal forebrain, Prog. Brain Res. 98 (1993) 31–49, https://doi.org/10.1016/s0079-6123(08)62379-1.

[21] W. Bondareff, C.Q. Mountjoy, M. Roth, M.N. Rossor, L.L. Iversen, G.P. Reynolds, D. L. Hauser, Neuronal degeneration in locus ceruleus and cortical correlates of Alzheimer disease, Alzheimer Dis. Assoc. Disord. 1 (1987) 256–262, https://doi.org/10.1097/00002093-198701040-00005.

[22] M. Heider, R. Schliebs, S. Rossner, V. Bigl, Basal forebrain cholinergic immunolesion by 192IgG-saporin: evidence for a presynaptic location of subpopulations of alpha 2- and beta-adrenergic as well as 5-HT2A receptors on cortical cholinergic terminals, Neurochem. Res. 22 (1997) 957–966, https://doi.org/10.1023/a:1022418708293.

[23] S. Tellez, F. Colpaert, M. Marien, Acetylcholine release in the rat prefrontal cortex in vivo: modulation by alpha 2-adrenoceptor agonists and antagonists, J. Neurochem. 68 (1997) 778–785, https://doi.org/10.1046/j.1471-4159.1997.68020778.x.

[24] S. Tellez, F. Colpaert, M. Marien, Alpha2-adrenoceptor modulation of cortical acetylcholine release in vivo, Neuroscience 89 (1999) 1041–1050, https://doi.org/10.1016/s0306-4522(98)00392-3.

[25] K.F. Manaye, P.R. Mouton, G. Xu, A. Drew, D.-L. Lei, Y. Sharma, G.W. Rebeck, S. Turner, Age-related loss of noradrenergic neurons in the brains of triple transgenic mice, Age (Dordr.) 35 (2013) 139–147, https://doi.org/10.1007/s11357-011-9343-0.

[26] S. Kalinin, P.E. Polak, S.X. Lin, A.J. Sakharkar, S.C. Pandey, D.L. Feinstein, The noradrenaline precursor L-DOPS reduces pathology in a mouse model of Alzheimer's disease, Neurobiol. Aging 33 (2012) 1651–1663, https://doi.org/10.1016/j.neurobiolaging.2011.04.012.

[27] P. Rizk, J. Salazar, R. Raisman-Vozari, M. Marien, M. Ruberg, F. Colpaert, T. Debeir, The alpha2-adrenoceptor antagonist dexefaroxan enhances hippocampal neurogenesis by increasing the survival and differentiation of new granule cells, Neuropsychopharmacol. Off. Publ. Am. Coll. Neuropsychopharmacol. 31 (2006) 1146–1157, https://doi.org/10.1038/sj.npp.1300954.

[28] M.M. Melkonyan, L. Hunanyan, A. Lourhmati, N. Layer, S. Beer-Hammer, K. Yenkoyan, M. Schwab, L. Danielyan, Neuroprotective, neurogenic, and amyloid beta reducing effect of a novel alpha 2-adrenoblocker, mesedin, on astroglia and neuronal progenitors upon hypoxia and glutamate exposure, Int. J. Mol. Sci. 19 (2017), https://doi.org/10.3390/ijms19010009.

[29] R. Pintus, M. Riggi, C. Cannarozzo, A. Valeri, G. de Leo, M. Romano, R. Gulino, G. Leanza, Essential role of hippocampal noradrenaline in the regulation of spatial working memory and TDP-43 tissue pathology, J. Comp. Neurol. 526 (2018) 1131–1147, https://doi.org/10.1002/cne.24397.

[30] D. Impellizzeri, R. Siracusa, M. Cordaro, R. Crupi, A.F. Peritore, E. Gugliandolo, R. D'Amico, S. Petrosino, M. Evangelista, R. Di Paola, S. Cuzzocrea, N-Palmitoylethanolamine-oxazoline (PEA-OXA): A new therapeutic strategy to reduce neuroinflammation, oxidative stress associated to vascular dementia in an experimental model of repeated bilateral common carotid arteries occlusion, Neurobiol. Dis. 125 (2019) 77–91, https://doi.org/10.1016/j.nbd.2019.01.007.

[31] S. Boccella, F. Guida, M. Iannotta, F.A. Iannotti, R. Infantino, F. Ricciardi, C. Cristiano, R.M. Vitale, P. Amodeo, I. Marabese, C. Belardo, V. de Novellis, S. Paino, E. Palazzo, A. Calignano, V. Di Marzo, S. Maione, L. Luongo, 2-Pentadecyl-2-oxazoline ameliorates memory impairment and depression-like behaviour in neuropathic mice: possible role of adrenergic alpha2- and H3 histamine autoreceptors, Mol. Brain. 14 (2021) 28, https://doi.org/10.1186/s13041-020-00724-z.

[32] S. Boccella, M. Iannotta, C. Cristiano, F.A. Iannotti, F. Del Bello, F. Guida, C. Belardo, R. Infantino, F. Ricciardi, M. Giannella, A. Calignano, V. Di Marzo, S. Maione, L. Luongo, Treatment with 2-pentadecyl-2-oxazoline restores mild traumatic brain injury-induced sensorial and neuropsychiatric dysfunctions, Front. Pharmacol. 11 (2020) 91, https://doi.org/10.3389/fphar.2020.00091.

[33] S. Petrosino, M. Campolo, D. Impellizzeri, I. Paterniti, M. Allarà, E. Gugliandolo, R. D'Amico, R. Siracusa, M. Cordaro, E. Esposito, V. Di Marzo, S. Cuzzocrea, 2-Pentadecyl-2-oxazoline, the oxazoline of PEA, modulates carrageenan-induced acute inflammation, Front. Pharmacol. 8 (2017), https://doi.org/10.3389/fphar.2017.00308.

[34] H.Y. Kim, D.K. Lee, B.-R. Chung, H.V. Kim, Y. Kim, Intracerebroventricular injection of amyloid-β peptides in normal mice to acutely induce alzheimer-like cognitive deficits, J. Vis. Exp. (2016), https://doi.org/10.3791/53308.

[35] E. Mhillaj, M.G. Morgese, P. Tucci, A. Furiano, L. Luongo, M. Bove, S. Maione, V. Cuomo, S. Schiavone, L. Trabace, Celecoxib prevents cognitive impairment and neuroinflammation in soluble amyloid β-treated rats, Neuroscience 372 (2018) 58–73, https://doi.org/10.1016/j.neuroscience.2017.12.046.

[36] P. Tucci, E. Mhillaj, M.G. Morgese, M. Colaianna, M. Zotti, S. Schiavone, M. Cicerale, V. Trezza, P. Campolongo, V. Cuomo, L. Trabace, Memantine prevents memory consolidation failure induced by soluble beta amyloid in rats, Front. Behav. Neurosci. 8 (2014) 332, https://doi.org/10.3389/fnbeh.2014.00332.

[37] E.F. Pettersen, T.D. Goddard, C.C. Huang, G.S. Couch, D.M. Greenblatt, E.C. Meng, T.E. Ferrin, UCSF Chimera–a visualization system for exploratory research and analysis, J. Comput. Chem. 25 (2004) 1605–1612, https://doi.org/10.1002/jcc.20084.

[38] G.M. Morris, R. Huey, W. Lindstrom, M.F. Sanner, R.K. Belew, D.S. Goodsell, A. J. Olson, AutoDock4 and AutoDockTools4: automated docking with selective receptor flexibility. J. Comput. Chem. 30 (2009) 2785–2791, https://doi.org/10.1002/jcc.21256.

[39] O. Trott, A.J. Olson, AutoDock Vina: improving the speed and accuracy of docking with a new scoring function, efficient optimization, and multithreading. J. Comput. Chem. 31 (2010) 455–461, https://doi.org/10.1002/jcc.21334.

[40] N. Eswar, B. Webb, M.A. Marti-Renom, M.S. Madhusudhan, D. Eramian, M.-Y. Shen, U. Pieper, A. Sali, Comparative protein structure modeling using Modeller. Curr. Protoc. Bioinforma. Chapter 5 Unit 5-6 (2006) https://doi.org/10.1002/0471250953.bi0506s15.

[41] F.A. Iannotti, F. De Maio, E. Panza, G. Appendino, O. Taglialatela-Scafati, L. De Petrocellis, P. Amodeo, R.M. Vitale, Identification and characterization of cannabimovone, a cannabinoid from Cannabis sativa, as a novel PPARγ agonist via a combined computational and functional study, Molecules 25 (2020), https://doi.org/10.3390/molecules25051119.

[42] D.A. Case, K. Belfon, I.Y. Ben-Shalom, S.R. Brozell, D.S. Cerutti, T.E. Cheatham III, V.W.D. Cruzeiro, T.A. Darden, R.E. Duke, G. Giambasu, M.K. Gilson, H. Gohlke, A. W. Goetz, R. Harris, S. Izadi, S.A. Izmailov, K. Kasavajhala, A. Kovalenko, R. Krasny, T. Kurtzman, T.S. Lee, S. LeGrand, P. Li, C. Lin, J. Liu, T. Luchko, R. Luo, V. Man, K.M. Merz, Y. Miao, O. Mikhailovskii, H. Nguyen, A. Onufriev, F. Pan, S. Pantano, R. Qi, D.R. Roe, A. Roitberg, C. Sagui, S. Schott-Verdugo, J. Shen, C. L. Simmerling, N.R. Skrynnikov, J. Smith, J. Swails, R.C. Walker, L. Wang, L. Wilson, R.M. Wolf, X. Wu, Y. Xiong, Y. Xue, D.M. York, P.A. Kollman, AMBER2020, University of California, San Francisco, 2020.

[43] F.K. Paxinos G, The mouse brain in stereotaxic coordinates, 2004.

[44] F. Guida, M. Iannotta, G. Misso, F. Ricciardi, S. Boccella, V. Tirino, M. Falco, V. Desiderio, R. Infantino, G. Pieretti, V. de Novellis, G. Papaccio, L. Luongo, M. Caraglia, S. Maione, Long-term neuropathic pain behaviors correlate with synaptic plasticity and limbic circuit alteration: a comparative observational study in mice, Pain 163 (2022) 1590–1602, https://doi.org/10.1097/j.pain.0000000000002549.

[45] A. Wolf, B. Bauer, E.L. Abner, T. Ashkenazy-Frolinger, A.M.S. Hartz, A comprehensive behavioral test battery to assess learning and memory in 129S6/Tg2576 mice, PLoS One 11 (2016), e0147733, https://doi.org/10.1371/journal.pone.0147733.

[46] C. Belardo, M. Iannotta, S. Boccella, R.C. Rubino, F. Ricciardi, R. Infantino, G. Pieretti, L. Stella, S. Paino, I. Marabese, R. Maisto, L. Luongo, S. Maione, F. Guida, Oral Cannabidiol prevents allodynia and neurological dysfunctions in a mouse model of mild traumatic brain injury, Front. Pharmacol. 10 (2019) 352, https://doi.org/10.3389/fphar.2019.00352.
[47] M.J. Wayner, D.L. Armstrong, C.F. Phelix, Y. Oomura, Orexin-A (Hypocretin-1) and leptin enhance LTP in the dentate gyrus of rats in vivo, Peptides 25 (2004) 991–996, https://doi.org/10.1016/j.peptides.2004.03.018.
[48] R. Infantino, C. Schiano, L. Luongo, S. Paino, G. Mansueto, S. Boccella, F. Guida, F. Ricciardi, M. Iannotta, C. Belardo, I. Marabese, G. Pieretti, N. Serra, C. Napoli, S. Maione, MED1/BDNF/TrkB pathway is involved in thalamic hemorrhage-induced pain and depression by regulating microglia, Neurobiol. Dis. 164 (2022), 105611, https://doi.org/10.1016/j.nbd.2022.105611.
[49] P. Chomczynski, N. Sacchi, Single-step method of RNA isolation by acid guanidinium thiocyanate-phenol-chloroform extraction, Anal. Biochem. 162 (1987) 156–159, https://doi.org/10.1006/abio.1987.9999.
[50] N. Maggio, S. Sellitti, C.P. Capano, M. Papa, Tissue-transglutaminase in rat and human brain: light and electron immunocytochemical analysis and in situ hybridization study, Brain Res. Bull. 56 (2001) 173–182, https://doi.org/10.1016/s0361-9230(01)00649-9.
[51] Y. Chen, Y. Peng, P. Che, M. Gannon, Y. Liu, L. Li, G. Bu, T. van Groen, K. Jiao, Q. Wang, α(2A) adrenergic receptor promotes amyloidogenesis through disrupting APP-SorLA interaction, Proc. Natl. Acad. Sci. USA 111 (2014) 17296–17301, https://doi.org/10.1073/pnas.1409513111.
[52] D.A. Horstman, S. Brandon, A.L. Wilson, C.A. Guyer, E.J.J. Cragoe, L.E. Limbird, An aspartate conserved among G-protein receptors confers allosteric regulation of alpha 2-adrenergic receptors by sodium. J. Biol. Chem. 265 (1990) 21590–21595.
[53] H.J. Motulsky, P.A. Insel, Influence of sodium on the alpha 2-adrenergic receptor system of human platelets. Role for intraplatelet sodium in receptor binding, J. Biol. Chem. 258 (1983) 3913–3919.
[54] V. Katritch, G. Fenalti, E.E. Abola, B.L. Roth, V. Cherezov, R.C. Stevens, Allosteric sodium in class A GPCR signaling, Trends Biochem. Sci. 39 (2014) 233–244, https://doi.org/10.1016/j.tibs.2014.03.002.
[55] Y. Vyas, J.M. Montgomery, J.E. Cheyne, Hippocampal deficits in amyloid-β-related rodent models of alzheimer's disease, Front. Neurosci. 14 (2020) 266, https://doi.org/10.3389/fnins.2020.00266.
[56] M. Gannon, Q. Wang, Complex noradrenergic dysfunction in Alzheimer's disease: low norepinephrine input is not always to blame, Brain Res. 2019 (1702) 12–16, https://doi.org/10.1016/j.brainres.2018.01.001.
[57] M.M. Uys, M. Shahid, B.H. Harvey, Therapeutic potential of selectively targeting the α(2C)-adrenoceptor in cognition, depression, and schizophrenia-new developments and future perspective, Front. Psychiatry 8 (2017) 144, https://doi.org/10.3389/fpsyt.2017.00144.
[58] A.K. Evans, P.M. Ardestani, B. Yi, H.H. Park, R.K. Lam, M. Shamloo, Beta-adrenergic receptor antagonism is proinflammatory and exacerbates neuroinflammation in a mouse model of Alzheimer's Disease, Neurobiol. Dis. 146 (2020), 105089, https://doi.org/10.1016/j.nbd.2020.105089.
[59] V.S. Ramasamy, M. Samidurai, H.J. Park, M. Wang, R.Y. Park, S.Y. Yu, H.K. Kang, S. Hong, W.-S. Choi, Y.Y. Lee, H.-S. Kim, J. Jo, Avenanthramide-C Restores Impaired Plasticity and Cognition in Alzheimer's Disease Model Mice, Mol. Neurobiol. 57 (2020) 315–330, https://doi.org/10.1007/s12035-019-01707-5.
[60] M.R. Hynd, H.L. Scott, P.R. Dodd, Glutamate-mediated excitotoxicity and neurodegeneration in Alzheimer's disease, Neurochem. Int. 45 (2004) 583–595, https://doi.org/10.1016/j.neuint.2004.03.007.
[61] S.M. Stahl, Beyond the dopamine hypothesis of schizophrenia to three neural networks of psychosis: dopamine, serotonin, and glutamate, CNS Spectr. 23 (2018) 187–191, https://doi.org/10.1017/S1092852918001013.
[62] G.A. Czapski, J.B. Strosznajder, Glutamate and GABA in microglia-neuron cross-talk in alzheimer's disease, Int. J. Mol. Sci. 22 (2021), https://doi.org/10.3390/ijms222111677.
[63] L.S. Kegeles, Brain GABA Function and Psychosis. Am. J. Psychiatry 173 (2016) 448–449, https://doi.org/10.1176/appi.ajp.2016.16020165.
[64] C. Belardo, N. Alessio, M. Pagano, E. De Dominicis, R. Infantino, M. Perrone, M. Iannotta, U. Galderisi, B. Rinaldi, D. Scuteri, G. Bagetta, E. Palazzo, S. Maione, L. Luongo, PEA-OXA ameliorates allodynia, neuropsychiatric and adipose tissue remodeling induced by social isolation, Neuropharmacology 208 (2022), 108978, https://doi.org/10.1016/j.neuropharm.2022.108978.
[65] J.A. Ross, B.A.S. Reyes, E.J.Van Bockstaele, Amyloid beta peptides, locus coeruleus-norepinephrine system and dense core vesicles, Brain Res. 2019 (1702) 46–53, https://doi.org/10.1016/j.brainres.2018.03.009.
[66] M. Gannon, Y. Peng, K. Jiao, Q. Wang, The α2 adrenergic receptor as a novel target for alzheimer's disease, FASEB J. 30 (2016), https://doi.org/10.1096/fasebj.30.1_supplement.707.2 (707.2-707.2).
[67] M. Haglund, M. Sjöbeck, E. Englund, Locus ceruleus degeneration is ubiquitous in Alzheimer's disease: possible implications for diagnosis and treatment, Neuropathology 26 (2006) 528–532, https://doi.org/10.1111/j.1440-1789.2006.00725.x.
[68] M.A. Raskind, E.R. Peskind, Neurobiologic bases of noncognitive behavioral problems in Alzheimer disease, Alzheimer Dis. Assoc. Disord. 8 Suppl 3 (1994) 54–60.
[69] L.Y. Wang, J.B. Shofer, K. Rohde, K.L. Hart, D.J. Hoff, Y.H. McFall, M.A. Raskind, E.R. Peskind, Prazosin for the treatment of behavioral symptoms in patients with Alzheimer disease with agitation and aggression, Am. J. Geriatr. Psychiatry . J. Am. Assoc. Geriatr. Psychiatry 17 (2009) 744–751, https://doi.org/10.1097/JGP.0b013e3181ab8c61.
[70] N. Herrmann, K.L. Lanctôt, L.R. Khan, The role of norepinephrine in the behavioral and psychological symptoms of dementia, J. Neuropsychiatry Clin. Neurosci. 16 (2004) 261–276, https://doi.org/10.1176/jnp.16.3.261.
[71] V. Chan-Palay, E. Asan, Alterations in catecholamine neurons of the locus coeruleus in senile dementia of the Alzheimer type and in Parkinson's disease with and without dementia and depression, J. Comp. Neurol. 287 (1989) 373–392, https://doi.org/10.1002/cne.902870308.
[72] U. Rüb, K. Del Tredici, C. Schultz, D.R. Thal, E. Braak, H. Braak, The autonomic higher order processing nuclei of the lower brain stem are among the early targets of the Alzheimer's disease-related cytoskeletal pathology, Acta Neuropathol. 101 (2001) 555–564, https://doi.org/10.1007/s004010000320.
[73] R.S. Wilson, S. Nag, P.A. Boyle, L.P. Hizel, L. Yu, A.S. Buchman, J.A. Schneider, D. A. Bennett, Neural reserve, neuronal density in the locus ceruleus, and cognitive decline, Neurology 80 (2013) 1202–1208, https://doi.org/10.1212/WNL.0b013e3182897103.
[74] T. Arendt, M.K. Brückner, M. Morawski, C. Jäger, H.-J. Gertz, Early neurone loss in Alzheimer's disease: cortical or subcortical? Acta Neuropathol. Commun. 3 (2015) 10, https://doi.org/10.1186/s40478-015-0187-1.
[75] P.J. Dolan, G.V.W. Johnson, The role of tau kinases in Alzheimer's disease, Curr. Opin. Drug Discov. Dev. 13 (2010) 595–603.
[76] F. Zhang, M. Gannon, Y. Chen, S. Yan, S. Zhang, W. Feng, J. Tao, B. Sha, Z. Liu, T. Saito, T. Saido, C.D. Keene, K. Jiao, E.D. Roberson, H. Xu, Q. Wang, β-amyloid redirects norepinephrine signaling to activate the pathogenic GSK3β/tau cascade, Sci. Transl. Med. 12 (2020), https://doi.org/10.1126/scitranslmed.aay6931.
[77] J.R. Muñoz-Montaño, F.J. Moreno, J. Avila, J. Diaz-Nido, Lithium inhibits Alzheimer's disease-like tau protein phosphorylation in neurons, FEBS Lett. 411 (1997) 183–188, https://doi.org/10.1016/s0014-5793(97)00688-1.
[78] M. Hong, D.C. Chen, P.S. Klein, V.M. Lee, Lithium reduces tau phosphorylation by inhibition of glycogen synthase kinase-3. J. Biol. Chem. 272 (1997) 25326–25332, https://doi.org/10.1074/jbc.272.40.25326.
[79] C. Hooper, R. Killick, S. Lovestone, The GSK3 hypothesis of Alzheimer's disease, J. Neurochem. 104 (2008) 1433–1439, https://doi.org/10.1111/j.1471-4159.2007.05194.x.
[80] J.B. Leverenz, M.A. Miller, D.J. Dobie, E.R. Peskind, M.A. Raskind, Increased alpha 2-adrenergic receptor binding in locus coeruleus projection areas in dementia with Lewy bodies, Neurobiol. Aging 22 (2001) 555–561, https://doi.org/10.1016/s0197-4580(01)00221-4.
[81] Y. Duan, J.J. Grady, P.C. Albertsen, Z. Helen Wu, Tamsulosin and the risk of dementia in older men with benign prostatic hyperplasia, Pharmacoepidemiol. Drug Saf. 27 (2018) 340–348, https://doi.org/10.1002/pds.4361.
[82] V.A.D. Holanda, M.C. Oliveira, E.D. da Silva Junior, E.C. Gavioli, Tamsulosin facilitates depressive-like behaviors in mice: Involvement of endogenous glucocorticoids, Brain Res. Bull. 178 (2022) 29–36, https://doi.org/10.1016/j.brainresbull.2021.11.005.
[83] S. Cao, D.W. Fisher, G. Rodriguez, T. Yu, H. Dong, Comparisons of neuroinflammation, microglial activation, and degeneration of the locus coeruleus-norepinephrine system in APP/PS1 and aging mice. J. Neuroinflamm. 18 (2021) 10, https://doi.org/10.1186/s12974-020-02054-2.
[84] K. Mori, E. Ozaki, B. Zhang, L. Yang, A. Yokoyama, I. Takeda, N. Maeda, M. Sakanaka, J. Tanaka, Effects of norepinephrine on rat cultured microglial cells that express alpha1, alpha2, beta1 and beta2 adrenergic receptors, Neuropharmacology 43 (2002) 1026–1034, https://doi.org/10.1016/s0028-3908(02)00211-3.
[85] M.T. Heneka, M.J. Carson, J. El Khoury, G.E. Landreth, F. Brosseron, D.L. Feinstein, A.H. Jacobs, T. Wyss-Coray, J. Vitorica, R.M. Ransohoff, K. Herrup, S.A. Frautschy, B. Finsen, G.C. Brown, A. Verkhratsky, K. Yamanaka, J. Koistinaho, E. Latz, A. Halle, G.C. Petzold, T. Town, D. Morgan, M.L. Shinohara, V.H. Perry, C. Holmes, N.G. Bazan, D.J. Brooks, S. Hunot, B. Joseph, N. Deigendesch, O. Garaschuk, E. Boddeke, C.A. Dinarello, J.C. Breitner, G.M. Cole, D.T. Golenbock, M. P. Kummer, Neuroinflammation in Alzheimer's disease, Lancet Neurol. 14 (2015) 388–405, https://doi.org/10.1016/S1474-4422(15)70016-5.
[86] S. Boccella, C. Cristiano, R. Romano, M. Iannotta, C. Belardo, A. Farina, F. Guida, F. Piscitelli, E. Palazzo, M. Mazzitelli, R. Imperatore, L. Tunisi, V. de Novellis, L. Cristino, V. Di Marzo, A. Calignano, S. Maione, L. Luongo, Ultra-micronized palmitoylethanolamide rescues the cognitive decline-associated loss of neural plasticity in the neuropathic mouse entorhinal cortex-dentate gyrus pathway, Neurobiol. Dis. 121 (2019) 106–119, https://doi.org/10.1016/j.nbd.2018.09.023.
[87] S.Y. Kim, P. Grant, J.H. Lee, H.C. Pant, P.M. Steinert, Differential expression of multiple transglutaminases in human brain. Increased expression and cross-linking by transglutaminases 1 and 2 in Alzheimer's disease, J. Biol. Chem. 274 (1999) 30715–30721, https://doi.org/10.1074/jbc.274.43.30715.
[88] J. Zhang, H. Grosso Jasutkar, R. Yan, J.-M. Woo, K.-W. Lee, J.-Y. Im, E. Junn, S. E. Iismaa, M.M. Mouradian, Transglutaminase 2 depletion attenuates α-synuclein mediated toxicity in mice, Neuroscience 441 (2020) 58–64, https://doi.org/10.1016/j.neuroscience.2020.05.047.
[89] N.G. Gatta, A. Parente, F. Guida, S. Maione, V. Gentile, Neuronutraceuticals modulate lipopolysaccharide- or amyloid-β 1-42 peptide-induced transglutaminase 2 overexpression as a marker of neuroinflammation in mouse microglial cells, Appl. Sci. 11 (2021), https://doi.org/10.3390/app11125718.
[90] B.A. Citron, Z. Suo, K. SantaCruz, P.J.A. Davies, F. Qin, B.W. Festoff, Protein crosslinking, tissue transglutaminase, alternative splicing and neurodegeneration, Neurochem. Int. 40 (2002) 69–78, https://doi.org/10.1016/s0197-0186(01)00062-6.
[91] J. Rudlong, A. Cheng, G.V.W. Johnson, The role of transglutaminase 2 in mediating glial cell function and pathophysiology in the central nervous system, Anal. Biochem. 591 (2020), 113556, https://doi.org/10.1016/j.ab.2019.113556.

[92] B. Min, K.C. Chung, New insight into transglutaminase 2 and link to neurodegenerative diseases, BMB Rep. 51 (2018) 5–13, https://doi.org/10.5483/bmbrep.2018.51.1.227.
[93] Z. Cai, M.D. Hussain, L.-J. Yan, Microglia, neuroinflammation, and beta-amyloid protein in Alzheimer's disease, Int. J. Neurosci. 124 (2014) 307–321, https://doi.org/10.3109/00207454.2013.833510.
[94] E.E. Tuppo, H.R. Arias, The role of inflammation in Alzheimer's disease, Int. J. Biochem. Cell Biol. 37 (2005) 289–305, https://doi.org/10.1016/j.biocel.2004.07.009.
[95] R.K. Shahidehpour, R.E. Higdon, N.G. Crawford, J.H. Neltner, E.T. Ighodaro, E. Patel, D. Price, P.T. Nelson, A.D. Bachstetter, Dystrophic microglia are associated with neurodegenerative disease and not healthy aging in the human brain, Neurobiol. Aging 99 (2021) 19–27, https://doi.org/10.1016/j.neurobiolaging.2020.12.003.
[96] D. Punzo, F. Errico, L. Cristino, S. Sacchi, S. Keller, C. Belardo, L. Luongo, T. Nuzzo, R. Imperatore, E. Florio, V. De Novellis, O. Affinito, S. Migliarini, G. Maddaloni, M. J. Sisalli, M. Pasqualetti, L. Pollegioni, S. Maione, L. Chiariotti, A. Usiello, Age-related changes in D-aspartate oxidase promoter methylation control extracellular D-aspartate levels and prevent precocious cell death during brain aging, J. Neurosci. 36 (2016) 3064–3078, https://doi.org/10.1523/JNEUROSCI.3881-15.2016.
[97] C. De Luca, L. Savarese, A.M. Colangelo, M.R. Bianco, G. Cirillo, L. Alberghina, M. Papa, Astrocytes and microglia-mediated immune response in maladaptive plasticity is differently modulated by NGF in the ventral horn of the spinal cord following peripheral nerve injury, Cell. Mol. Neurobiol. 36 (2016) 37–46, https://doi.org/10.1007/s10571-015-0218-2.
[98] A. Virtuoso, A.M. Colangelo, N. Maggio, U. Fennig, N. Weinberg, M. Papa, C. De Luca, The spatiotemporal coupling: regional energy failure and aberrant proteins in neurodegenerative diseases, Int. J. Mol. Sci. 22 (2021), https://doi.org/10.3390/ijms222111304.